Multidecadal Ocean Temperature and Salinity Variability in the Tropical North Atlantic: Linking with the AMO, AMOC, and Subtropical Cell

CHUNZAI WANG

NOAA/Atlantic Oceanographic and Meteorological Laboratory, Miami, Florida

LIPING ZHANG

Cooperative Institute for Marine and Atmospheric Studies, University of Miami, and NOAA/Atlantic Oceanographic and Meteorological Laboratory, Miami, Florida

(Manuscript received 1 October 2012, in final form 14 February 2013)

ABSTRACT

The Atlantic multidecadal oscillation (AMO) is characterized by the sea surface warming (cooling) of the entire North Atlantic during its warm (cold) phase. Both observations and most of the phase 5 of the Coupled Model Intercomparison Project (CMIP5) models also show that the warm (cold) phase of the AMO is associated with a surface warming (cooling) and a subsurface cooling (warming) in the tropical North Atlantic (TNA). It is further shown that the warm phase of the AMO corresponds to a strengthening of the Atlantic meridional overturning circulation (AMOC) and a weakening of the Atlantic subtropical cell (STC), which both induce an anomalous northward current in the TNA subsurface ocean. Because the mean meridional temperature gradient of the subsurface ocean is positive because of the temperature dome around 9°N, the advection by the anomalous northward current cools the TNA subsurface ocean during the warm phase of the AMO. The opposite is true during the cold phase of the AMO. It is concluded that the anticorrelated ocean temperature variation in the TNA associated with the AMO is caused by the meridional current variation induced by variability of the AMOC and STC, but the AMOC plays a more important role than the STC. Observations do not seem to show an obvious anticorrelated salinity relation between the TNA surface and subsurface oceans, but most of CMIP5 models simulate an out-of-phase salinity variation. Similar to the temperature variation, the mechanism is the salinity advection by the meridional current variation induced by the AMOC and STC associated with the AMO.

1. Introduction

One of the most important climate variations in the Atlantic is the Atlantic multidecadal oscillation (AMO), which is a basinwide mode in the entire North Atlantic and is defined by the North Atlantic sea surface temperature (SST) anomalies (e.g., Enfield et al. 2001; Knight et al. 2005). The AMO has significant regional and global climate associations, such as the northeast Brazilian and African Sahel rainfall (Folland et al. 1986; Rowell et al. 1995; Folland et al. 2001; Rowell 2003; Wang et al. 2012), the Atlantic warm pool (Wang et al. 2008; Zhang et al. 2012; Wang et al. 2013) and Atlantic hurricanes (Goldenberg et al. 2001; Wang and Lee 2009), and North American and European summer climate (Enfield et al. 2001; McCabe et al. 2004; Sutton and Hodson 2005). In spite of its importance, the mechanism of the AMO is still unclear. One of the most popular arguments is that the AMO is induced by the Atlantic meridional overturning circulation (AMOC) variations and associated heat transport fluctuations (Folland et al. 1986; Gray et al. 1997; Delworth and Mann 2000; Knight et al. 2005). Some of modeling studies indicate that the solar variability and/or volcanoes play a role in the AMO (Hansen et al. 2005; Otterå et al. 2003) or the external forcing aerosols can be as a primary driver for the AMO (Booth et al. 2012). A recent observational study shows that a positive feedback between the SST and dust aerosol in the North Atlantic via Sahel rainfall variability may be a mechanism for the AMO (Wang et al. 2012).

Corresponding author address: Dr. Liping Zhang, Physical Oceanography Division, NOAA/Atlantic Oceanographic and Meteorological Laboratory, 4301 Rickenbacker Causeway, Miami, FL 33149.
E-mail: liping.zhang@noaa.gov

DOI: 10.1175/JCLI-D-12-00721.1

As a basinwide SST mode in the North Atlantic, the AMO warming or cooling is also manifested in the tropical North Atlantic (TNA) SST anomalies. That is, the TNA SST variation on multidecadal time scales is in phase with the AMO. The variations of the TNA SST and upper-ocean temperature are very important because they directly affect hurricane activity in the North Atlantic (e.g., Shay et al. 2000; Wang et al. 2008). Here, we focus on the TNA ocean temperature variations associated with the AMO. Zhang (2007) and Wang et al. (2010) showed that the TNA SST anomalies are inversely related to or anticorrelated with the subsurface ocean temperature anomalies in association with the AMO. In other words, the TNA SST anomalies vary out of phase with the subsurface ocean temperature anomalies on multidecadal time scales. In a study for comparing several ocean reanalysis products by Corre et al. (2012), the variation of the TNA subsurface temperature with the AMO can also be seen (their Fig. 10). Zhang (2007) suggested that the anticorrelated change between the TNA surface and subsurface temperatures is a distinctive signature of the AMOC variation based on the coupled Geophysical Fluid Dynamics Laboratory Climate Model, version 2.0 (GFDL CM2.1) and thus can be taken as an AMOC fingerprint. The mechanism of the anticorrelated change proposed by Zhang (2007) is associated with the AMOC-induced TNA subsurface thermocline adjustment.

In the present paper, we further show that the anticorrelated multidecadal variation does exist in observational data and climate models of phase 5 of the Coupled Model Intercomparison Project (CMIP5). Using observational data and CMIP5 models, we demonstrate that the TNA subsurface cooling (warming) during the warm (cold) phase of the AMO is largely due to the meridional advection by the anomalous northward (southward) current, whereas the subsurface thermocline adjustment plays a secondary role. The present paper further shows that the anomalous northward (southward) current is attributed to variability of the AMOC and the shallow Atlantic subtropical cell (STC) (e.g., Malanotte-Rizzoli et al. 2000; Zhang et al. 2003). In addition, the paper also discusses variability of the TNA surface and subsurface salinity on multidecadal time scales.

The paper is organized as follows: Section 2 briefly introduces the datasets and methods used in this paper. The assessment of the anticorrelated multidecadal variation between TNA surface and subsurface temperatures in observational data and CMIP5 models is presented in section 3. The mechanisms of the anticorrelated multidecadal variation are analyzed and examined in section 4. Section 5 shows a linkage among the AMO, AMOC, STC, and TNA surface and subsurface ocean temperature variation. Section 6 briefly investigates the multidecadal variation of salinity in the TNA. The paper is concluded with a summary and discussion in section 7.

2. Datasets and methods

Several datasets are used in this study. The first one is the improved Extended Reconstructed SST (ERSST), with a 2° latitude by 2° longitude resolution (Smith and Reynolds 2004). The second dataset is the Simple Ocean Data Assimilation (SODA) (Carton and Giese 2008). The SODA uses an ocean general circulation model (GCM) to assimilate available temperature and salinity observations. The product is a gridded dataset of oceanic variables with monthly values at a 0.5° × 0.5° latitude–longitude horizontal resolution and 40 vertical levels (the SODA product is sometimes called observational data). The ocean model surface boundary conditions are taken from a new atmospheric dataset designated as the Twentieth Century Reanalysis version 2 (20CRv2), which contains the synoptic-observation-based estimate of global tropospheric variability spanning 1871–2008 at 6-hourly temporal and 2° spatial resolutions (Compo et al. 2011). The version 2.2.4 of the SODA data is used, with the time covering from 1871 to 2008. Additionally, the objectively analyzed temperature and salinity version 6.7 (Ishii et al. 2006) at 24 levels in the upper ocean of 1500 m from 1945 to 2010 is also used. The analysis is based on the World Ocean Database, the global temperature–salinity in the tropical Pacific from the Institut de Recherche pour le Développement (IRD), France, and the Centennial in situ Observation Based Estimates (COBE) SST. The Ishii et al. analysis also includes the Argo profiling buoy data in the final several years and the XBT depth bias correction.

Eighteen coupled GCM output datasets of the ''historical'' simulations provided to the Intergovernmental Panel on Climate Change (IPCC) Fifth Assessment Report (AR5) are also used in this study. The modeling center and country, IPCC model name, and temporal coverage are shown in Table 1. The model data can be downloaded from the website of CMIP5 (Taylor et al. 2012) (http://cmip-pcmdi.llnl.gov/cmip5/). The historical runs are forced by observed atmospheric composition changes which reflect both anthropogenic (greenhouse gases) and natural sources (volcanic influences, solar forcing, aerosols, and emissions of short-lived species and their precursors) and, for the first time, including time-evolving land cover. The historical runs cover much of the industrial period from the mid-nineteenth century to the present and are sometimes referred to as twentieth-century simulations. All of the coupled GCMs

TABLE 1. The 18 CMIP5 models used in this study.

Sponsor, country	Model name	Model expansion	Temporal coverage
Beijing Climate Center (BCC), China	BCC-CSM1–1	Beijing Climate Center, Climate System Model, 1-1	January 1850–December 2012
Canadian Centre for Climate Modeling and Analysis, Canada	CanESM2	Canadian Earth System Model, version 2	January 1850–December 2005
National Center for Atmospheric Research (NCAR), United States	CCSM4	Community Climate System Model, version 4	January 1850–December 2005
Météo-France/Centre National de Recherches Météorologiques (CNRM), France	CNRM-CM5	Centre National de Recherches Météorologiques Coupled Global Climate Model, version 5	January 1850–December 2005
Commonwealth Scientific and Industrial Research Organization (CSIRO), Australia	CSIRO Mk3.6.0	Commonwealth Scientific and Industrial Research Organisation Mark, version 3.6.0	January 1850–December 2005
Institute of Atmospheric Physics, Chinese Academy of Sciences, China	FGOALS-g2	Flexible Global Ocean–Atmosphere–Land System Model gridpoint, version 2	January 1900–December 2005
U.S. Department of Commerce/National Oceanic and Atmospheric Administration (NOAA)/Geophysical Fluid Dynamics Laboratory (GFDL), United States	GFDL-ESM2G	Geophysical Fluid Dynamics Laboratory Earth System Model with GOLD ocean component	January 1861–December 2005
	GFDL-ESM2M	Geophysical Fluid Dynamics Laboratory Earth System Model with MOM4 ocean component	January 1861–December 2005
National Aeronautics and Space Administration (NASA)/Goddard Institute for Space Studies (GISS), United States	GISS-E2H	Goddard Institute for Space Studies Model E, coupled with the HYCOM ocean model	January 1850–December 2005
	GISS-E2-R	Goddard Institute for Space Studies Model E, coupled with Russell ocean model	January 1850–December 2005
Met Office Hadley Centre, United Kingdom	HadGEM2-ES	Hadley Centre Global Environmental Model, version 2 (Earth System)	December 1859–November 2005
Institute Pierre Simon Laplace (IPSL), France	IPSL-CM5A-LR	L'Institut Pierre-Simon Laplace Coupled Model, version 5, coupled with NEMO, low resolution	January 1850–December 2005
	IPSL-CM5A-MR	L'Institut Pierre-Simon Laplace Coupled Model, version 5, coupled with NEMO, mid resolution	January 1850–December 2005
Center for Climate System Research (University of Tokyo), National Institute for Environmental Studies, and Frontier Research Center for Global Change (JAMSTEC), Japan	MIROC5	Model for Interdisciplinary Research on Climate, version 5	January 1850–December 2005
	MIROC-ESM	Model for Interdisciplinary Research on Climate, Earth System Model	January 1850–December 2005
	MIROC-ESM-CHEM	Model for Interdisciplinary Research on Climate, Earth System Model, Chemistry Coupled	January 1850–December 2005
Max Planck Institute (MPI) for Meteorology, Germany	MPI-ESM-P	Max Planck Institute Earth System Model, paleo	January 1850–December 2005
Meteorological Research Institute (MRI), Japan	MRI-CGCM3	Meteorological Research Institute Coupled Atmosphere–Ocean General Circulation Model, version 3	January 1850–December 2005

are coupled freely without flux correction. Variables of surface heat flux, wind, temperature, salinity, and current are used in this study.

Several statistical methods are used in this study, such as the lead–lag correlation and linear regression. To demonstrate possible mechanisms of the surface and subsurface ocean temperature variations in the TNA, we conduct the heat budget analysis of the zonal mean temperature. The ocean heat budget analysis is based on the temperature equation in which the local temperature

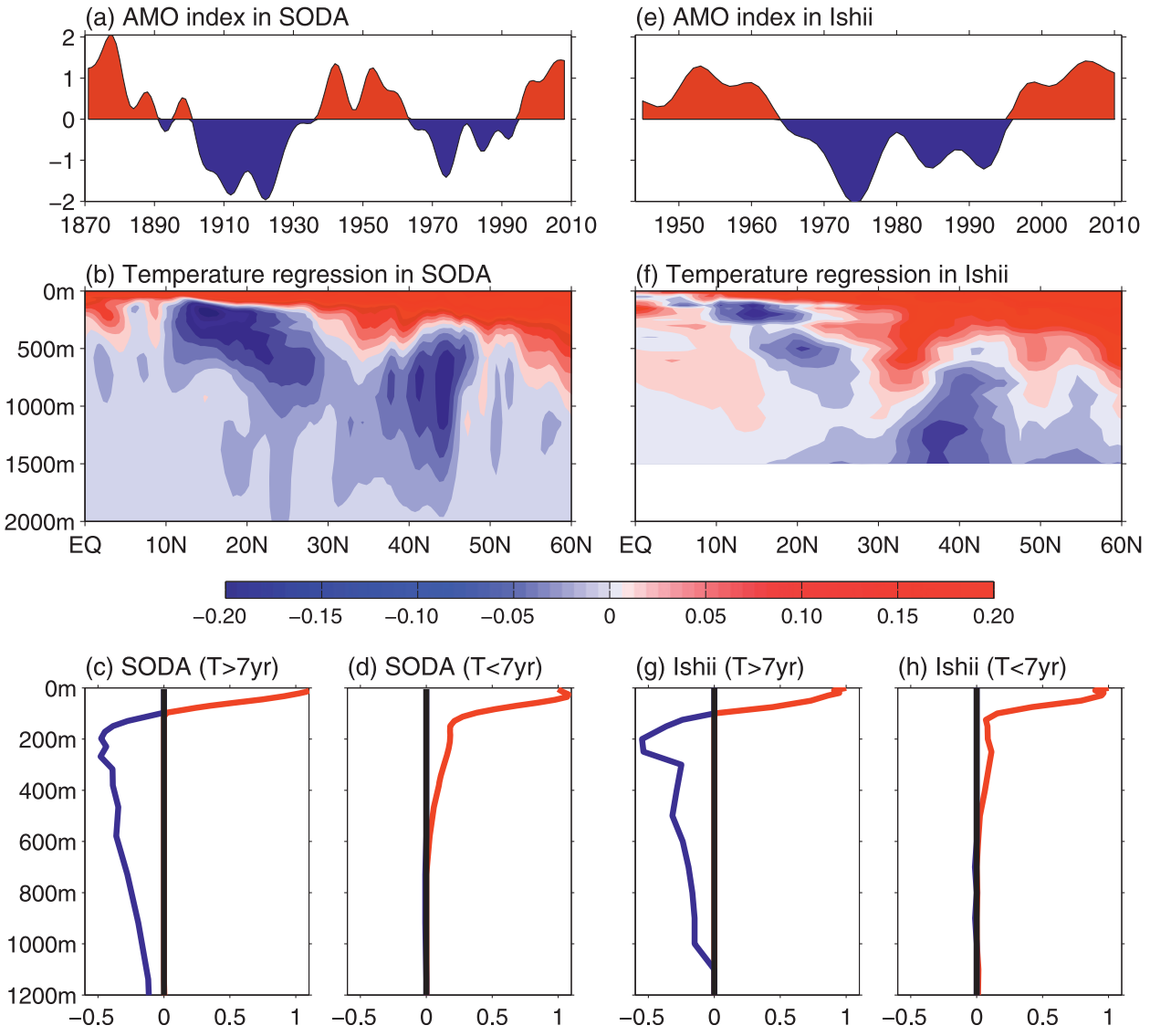

FIG. 1. Variations of ocean temperature in the North Atlantic. Shown are the normalized (by standard deviation) AMO index from the (a) SODA and (e) Ishii data, the regression (°C) of the Atlantic zonal mean temperature onto the normalized AMO index from the (b) SODA and (f) Ishii data, and regression (°C °C^{-1}) of the Atlantic temperature averaged in the region of 8°–20°N and coast to coast at each depth onto the SST on multidecadal (period of T higher than 7 yr) and interannual (period of T lower than 7 yr) time scales from the (c),(d) SODA data and (g),(h) Ishii data. The AMO is defined by the detrended SST anomalies averaged in the North Atlantic Ocean (0°–60°N, coast to coast) and smoothed by a 7-yr low-frequency filter.

change depends on ocean temperature advection terms and surface heat flux. Our major purpose is to qualitatively rather than quantitatively assess the relative importance of the surface heat flux and ocean advections in generating the low-frequency temperature variation. Since we focus on the zonal mean surface and subsurface temperature anomalies, the ocean advection in the zonal direction can be neglected. All the data are linearly detrended and smoothed by a 7-yr low-frequency filter (we use the fifth-order Butterworth low-pass filter).

3. Anticorrelated variation of TNA surface and subsurface ocean temperatures

a. Observed results

We first use the SODA and Ishii data to calculate the AMO indices (Figs. 1a,e) on low-frequency (or multidecadal) time scales. We then regress the Atlantic zonal mean ocean temperatures onto the multidecadal AMO indices (Figs. 1b,f). Consistent with the previous studies of Zhang (2007) and Wang et al. (2010), the TNA shows

an anticorrelated variation between the surface and subsurface temperatures on multidecadal time scales. It can be seen that the surface temperature is characterized by a basinwide and uniform warming (cooling) in the entire North Atlantic with a maximum magnitude occurring in the subpolar region during the warm (cold) phase of the AMO, in agreement with the definition of the AMO index. The penetration depth of the surface warming is latitude dependent. The higher the latitude is, the deeper the surface warming penetrates. On the contrary, the TNA subsurface ocean temperature tends to become cool (warm) during the warm (cold) phase of the AMO. In the TNA, the anomalous cooling appears below 100 m and penetrates down to 1500 m, with a maximum cooling around 200 m between 8° and 20°N. North of 20°N, the location of cooling anomaly becomes deeper.

The anticorrelated surface and subsurface temperature variation or vertical dipole temperature structure in the TNA occurs only on multidecadal time scales. The bottom panels of Fig. 1 show the regressions of the TNA ocean temperature anomalies at each depth onto the TNA SST anomalies (averaged in the region of 8°–20°N and coast to coast) on interannual and multidecadal time scales from the SODA and Ishii data. It is shown that the dipole structure in the TNA appears only on multidecadal time scales, whereas on interannual time scales the temperature profile exhibits a uniform positive regression between the surface and subsurface oceans. This suggests that the TNA dipole temperature anomaly should originate from the relatively slow ocean adjustment, particularly in the high latitudes, where the ocean has a long time memory.

To further demonstrate the anticorrelated variation, we plot the multidecadal time series of temperature anomalies at the sea surface and 200 m and vertically averaged temperature anomalies from 0 to 400 m using the SODA and Ishii data (Fig. 2). Since the Ishii data are available only from the middle of the twentieth century, for the purpose of consistency we plot both the time series starting from 1945. The anticorrelated or out-of-phase relationship between the SST anomalies and temperature anomalies at 200 m is obvious in both the datasets, with the correlation coefficients of −0.95 and −0.93 in the SODA and Ishii data, respectively. When the TNA surface ocean is warm (cold), the subsurface temperature at 200 m is cold (warm). Since the subsurface variation is deeper and larger than the surface (Figs. 1b,f), the vertically averaged temperature anomalies between 0 and 400 m mainly follow the subsurface temperature anomalies such as those at 200 m.

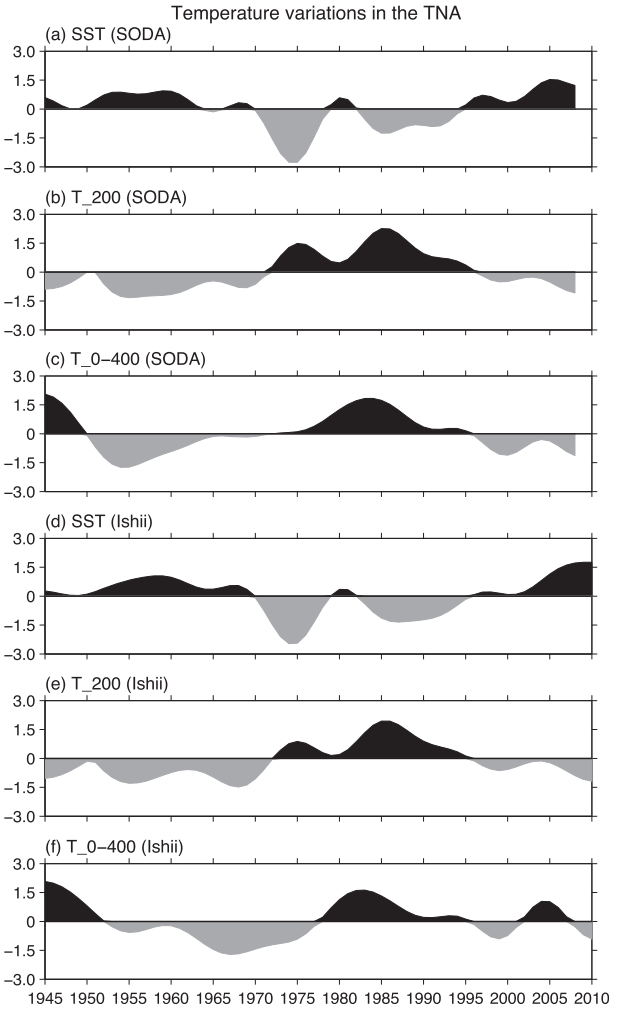

FIG. 2. Multidecadal time series of TNA (8°–20°N, coast to coast) ocean temperature anomalies at the sea surface and 200 m and vertically averaged temperature anomalies from 0 to 400 m using the (a)–(c) SODA and (d)–(f) Ishii data. All time series are normalized by their standard deviations.

b. CMIP5 simulations

The AMO indices from 18 CMIP5 model simulations and the ERSST observation are shown in Fig. 3. CMIP5 models show a significant decadal to multidecadal variation of the AMO; however, they strongly disagree in both phase and strength with the observation. To some degree, CMIP5 simulations share a relatively better resemblance with the observation than CMIP3 models (Medhaug and Furevik 2011), particularly in the last two decades. The two main discrepancies between the model and observation are during the early twentieth century (1900–20), when the models underestimate the cooling, and during the subsequent midcentury warming (1925–65), when the models are generally too cool. This could be due to errors in the observations, inadequacy in the modeled response to external forcing or forcing that is not included in model simulations, or different internal variations in different models. The contributions of external

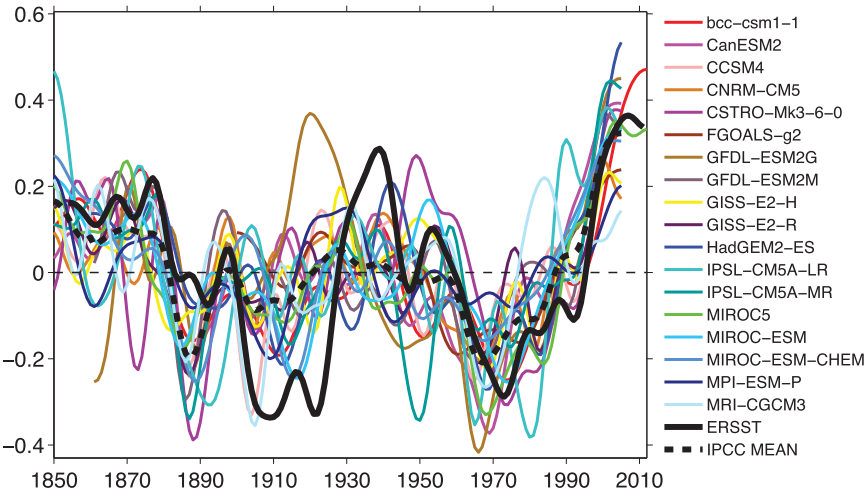

FIG. 3. The AMO indices in observation (ERSST) and CMIP5 models. The AMO index (°C) is calculated by the detrended SST anomalies averaged in the North Atlantic Ocean (0°–60°N, coast to coast) and smoothed by a 7-yr low-frequency filter.

forcing and internal variation to the North Atlantic SST in climate models are recently in debate (e.g., Ting et al. 2009; Booth et al. 2012; Terray 2012; Zhang et al. 2013). It is possible that a combination of both effects is attributed to the twentieth-century multidecadal SST variation in the North Atlantic; however, their relative importance remains an issue to be determined.

The regression of the Atlantic zonal mean temperatures onto the AMO index for individual models is shown in Fig. 4. Of 18 CMIP5 models, 12 models are able to simulate the anticorrelated variation between the TNA surface and subsurface ocean temperatures: BCC-CSM1–1, CanESM2, CNRM-CM5, CSIRO MK3.6.0, GFDL-ESM2G, GFDL-ESM2M, GISS-E2-R, HadGEM2-ES, MIROC5, MIROC-ESM-CHEM, MPI-ESM-P, and MRI-CGCM3 (Figs. 4a–l). These models simulate a surface warming (cooling) anomaly in the TNA and a subsurface cooling (warming) anomaly with the maximum around 200 m between 8° and 20°N during the warm (cold) phase of the AMO. The other six models do not well simulate the TNA subsurface cooling during the warm phase of the AMO: FGOALS-g2, GISS-E2H, IPSL-CM5A-LR, IPSL-CM5A-MR, MIROC-ESM, and CCSM4 (Figs. 1m–r). In the following section, we will examine physical mechanisms that are responsible for the vertical temperature dipole structure associated with the AMO.

4. Mechanisms of surface and subsurface ocean temperature variations

a. Long-term mean states

To help the understanding of the ocean temperature variations in the TNA, we first present the oceanic and atmospheric mean states in the TNA. Long-term mean surface net heat flux in the TNA is characterized by a heat loss from the ocean in the west and a heat gain in the east (Fig. 5a). The former is due to the strong trade wind–induced turbulent heat flux, whereas the latter is largely associated with the radiative heat flux. Surface freshwater flux (evaporation minus precipitation) exhibits a freshwater gain in the intertropical convergence zone (ITCZ) region (Fig. 5b), where the surface wind convergence is accompanied with the ascending motion. In the north of the ITCZ, the TNA is covered by a freshwater loss as a result of the surface wind divergence and the descending motion. Figure 5c displays the vertical structure of the zonal mean ocean temperature in the TNA region. In the surface, the temperature gradually decreases with the latitude, resulting from the solar radiation. Thus, the mean meridional SST gradient is negative near the surface, except near the equator because of the equatorial upwelling (Fig. 6a). In the subsurface, it is interesting to see that there is a temperature dome at 9°N, where the ITCZ is located and the isotherms on both sides tend to tilt upward (Fig. 5c). On the equatorward side of the temperature dome, the mean meridional temperature gradient in the subsurface ocean is negative, while the opposite is true on the poleward side (Fig. 6a). Similar to the temperature structure, the zonal mean salinity is also represented by a salinity dome at 9°N (Fig. 5d). Therefore, the mean meridional salinity gradient also features a dipole pattern across 9°N (Fig. 6b). In the surface, salinity is low in the ITCZ region and high in the subtropics (Fig. 5d) and thus gives rise to a positive meridional salinity gradient

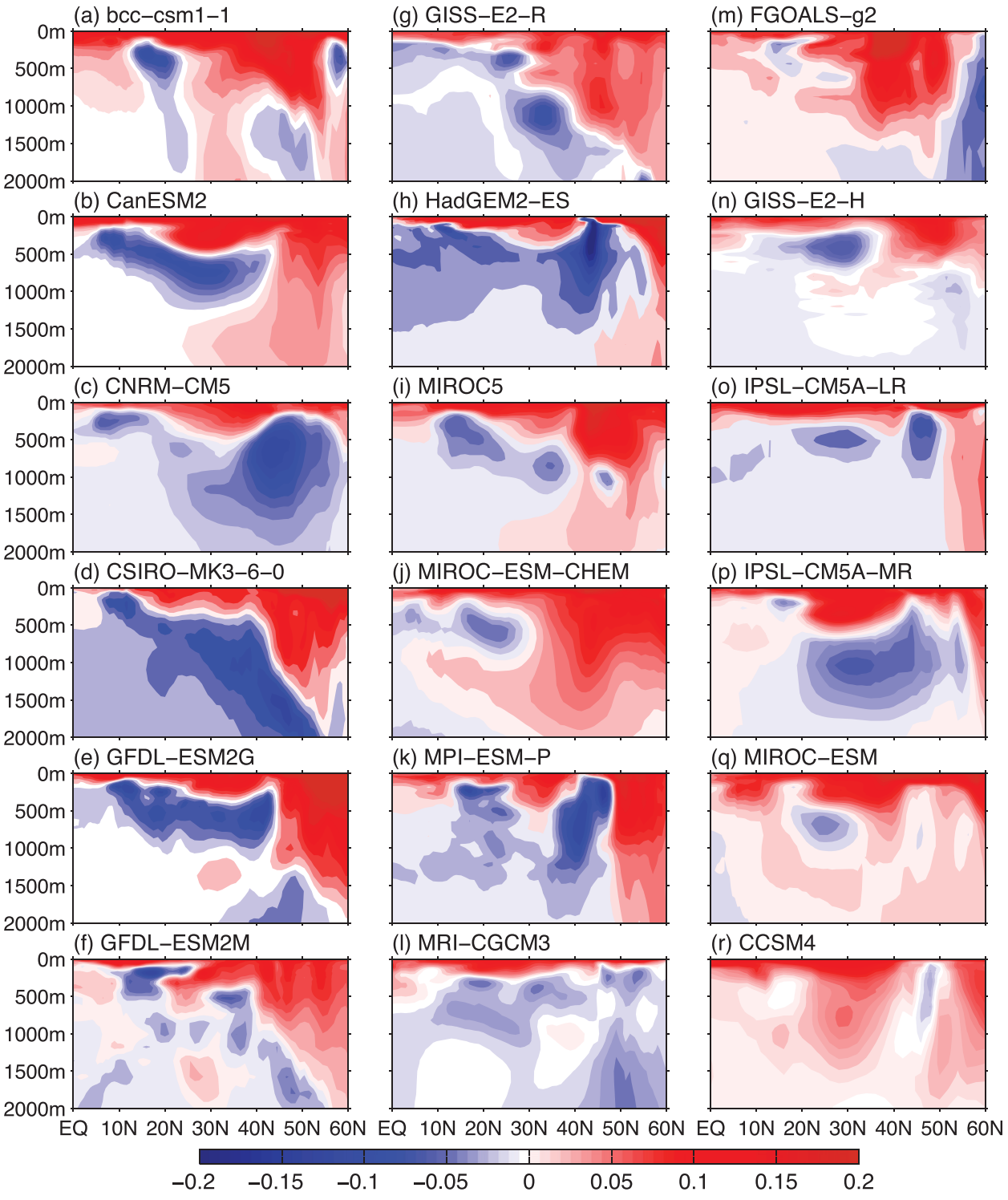

FIG. 4. Regression of the Atlantic zonal mean temperature (°C) onto the normalized AMO index from CMIP5 models.

north of the dome (Fig. 6b), which can be expected from the surface net freshwater flux (Fig. 5b). Further inspection finds that the maximum positive meridional temperature and salinity gradients in the subsurface locate in the depth of about 200 m between 8° and 16°N (Figs. 6a,b), which collocates with the maximum multidecadal subsurface TNA temperature variation (Fig. 1).

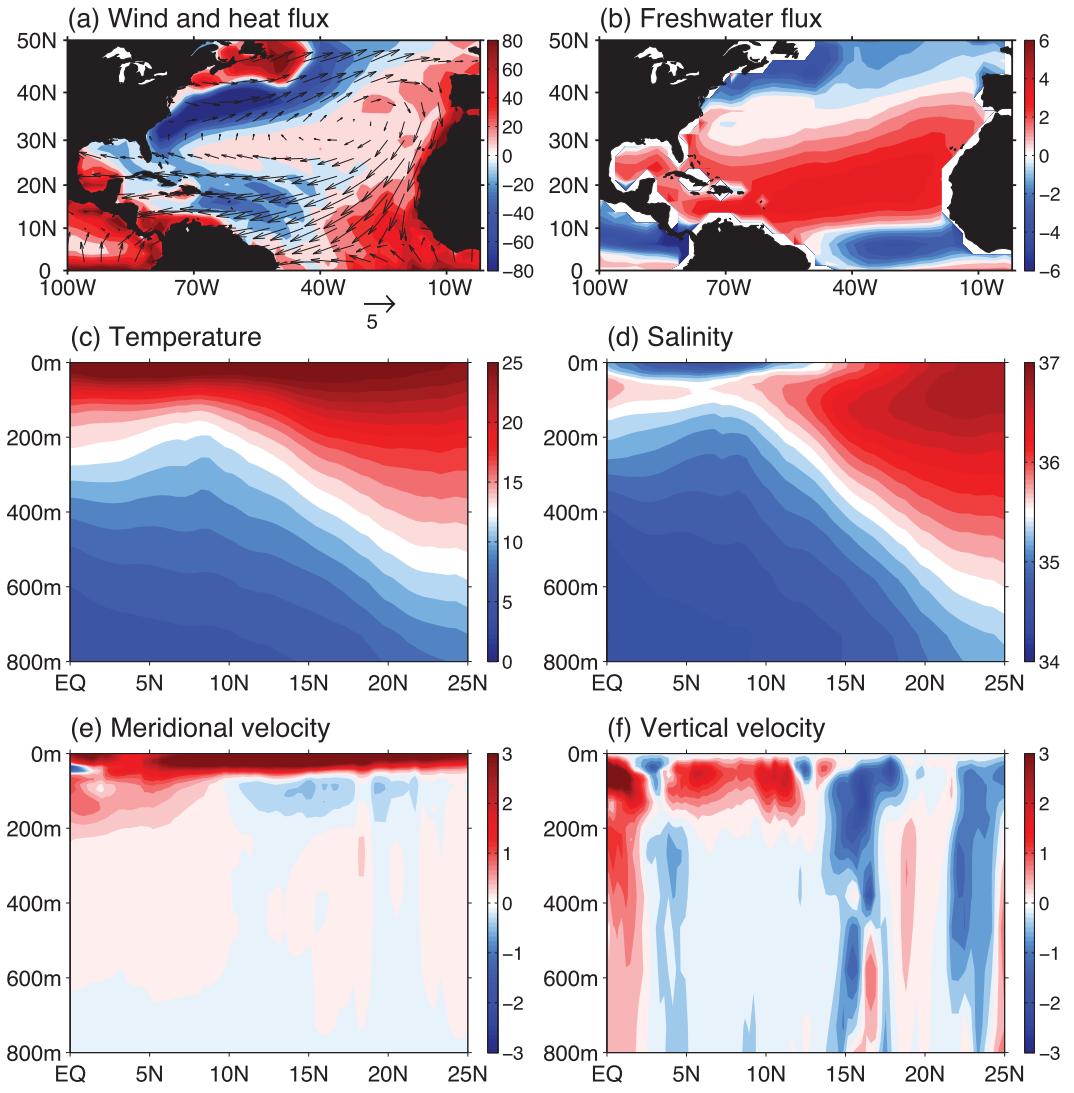

FIG. 5. Long-term mean background states in the TNA. The mean (a) surface wind ($m\,s^{-1}$) and net heat flux (positive downward; $W\,m^{-2}$) and (b) freshwater flux (evaporation minus precipitation; $mm\,day^{-1}$) are from the 20CRv2 data. The zonal (coast to coast) mean (c) temperature (°C), (d) salinity (psu), (e) meridional velocity ($10^{-2}\,m\,s^{-1}$), and (f) vertical velocity ($10^{-6}\,m\,s^{-1}$) are from the SODA data.

The vertical temperature gradient is always positive in the TNA with the maximum gradient in the upper layer from the equator to 15°N (Fig. 6c). Contrary to the temperature, there is a dipole structure in the vertical salinity gradient, with a negative gradient in the upper 100 m and a positive salinity gradient below (Fig. 6d). The surface negative salinity gradient can be attributed to the surface freshwater gain and the intrusion of subtropical high salinity in the subsurface (Fig. 5b). As expected, the zonal mean meridional ocean velocity displays a northward current above the Ekman layer, which results from the trade wind–induced northward Ekman drift (Fig. 5e). On the contrary, water tends to flow southward in the interior that can be explained by the Sverdrup relation. The zonal mean vertical ocean velocity in the TNA is generally characterized by an upwelling south of 14°N and a downwelling in the north (Fig. 5f), which is primarily due to the Ekman transport–induced vertical motion.

b. Physical mechanisms in observational data

We first examine the meridional and vertical advection terms contributing to the multidecadal subsurface temperature variation. Figure 7 shows the regression of various zonal mean terms onto the multidecadal AMO

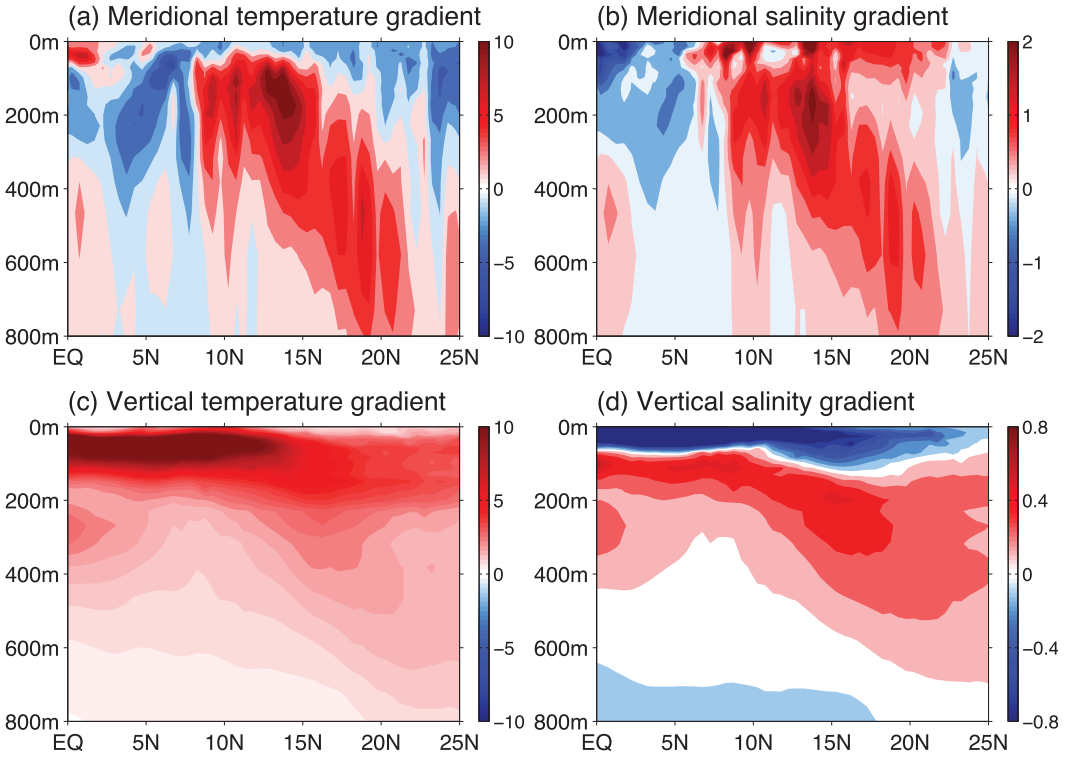

FIG. 6. Long-term mean (a) meridional temperature gradient (10^{-6} °C m^{-1}), (b) meridional salinity gradient (10^{-6} psu m^{-1}), (c) vertical temperature gradient (10^{-2} °C m^{-1}), and (d) vertical salinity gradient (10^{-2} psu m^{-1}) from the SODA data.

index in the SODA data (note that the Ishii data do not have ocean currents and cannot be used for the ocean heat budget). The similar results can be obtained by computing the zonal advection terms at each grid point and then performing the zonal mean and regression onto the AMO index. It is clearly seen that the TNA subsurface cooling anomalies can be broadly explained by the total meridional advection (Fig. 7a), while the total vertical advection plays a much smaller role except north of 14°N (Fig. 7e). The advection by the ocean currents is further decomposed into two components: anomalous (denoted by prime) and mean (denoted by overbar) currents. It is shown that the total meridional advection mainly arises from the advection by the anomalous meridional current ($-V'\partial\overline{T}/\partial y$; Fig. 7b), whereas the advection by the mean meridional current is secondary ($-\overline{V}\partial T'/\partial y$; Fig. 7c). Compared to these two terms, the nonlinear term is small ($-V'\partial T'/\partial y$; Fig. 7d). A remarkable feature is that the subsurface cooling between 8° and 20°N in Fig. 1b corresponds to the contribution due to the advection term by the anomalous current in Fig. 7b ($-V'\partial\overline{T}/\partial y<0$ in the TNA subsurface ocean). Because the mean meridional temperature gradient is positive at the TNA subsurface ocean ($\partial\overline{T}/\partial y>0$; Fig. 6a), an anomalous northward current must occur in the subsurface ocean: that is, V' must be positive. Since the zonally averaged field is considered here, it is expected that the anomalous northward current is associated with the flow variations of the AMOC and/or the Atlantic STC. We will come back this issue later.

Similar to the total meridional advection, the total vertical advection primarily depends on the advection by the anomalous vertical velocity (Fig. 7e versus Fig. 7f), while the advection by the mean vertical velocity plays a much smaller role (Fig. 7e versus Fig. 7g). The nonlinear term can be ignored (Fig. 7h). The advection by the anomalous vertical velocity ($-W'\partial\overline{T}/\partial z$) tends to cool temperature in the upper 400 m north of 14°N and to warm temperature south of 14°N. Because $\partial\overline{T}/\partial z$ is always positive, this implies that there is an anomalous downwelling (upwelling) south (north) of 14°N, consistent with the wind distribution (and its corresponded Ekman transport and vertical motion) associated with the AMO (Fig. 8a). The effect of the advection by the mean vertical velocity tends to be opposite to that by the anomalous vertical velocity (Fig. 7g versus Fig. 7f).

The contributions of both $-\overline{W}\partial T'/\partial z$ and $-\overline{V}\partial T'/\partial y$ to the TNA subsurface temperature cooling are small. These suggest that the anomalous temperature gradients

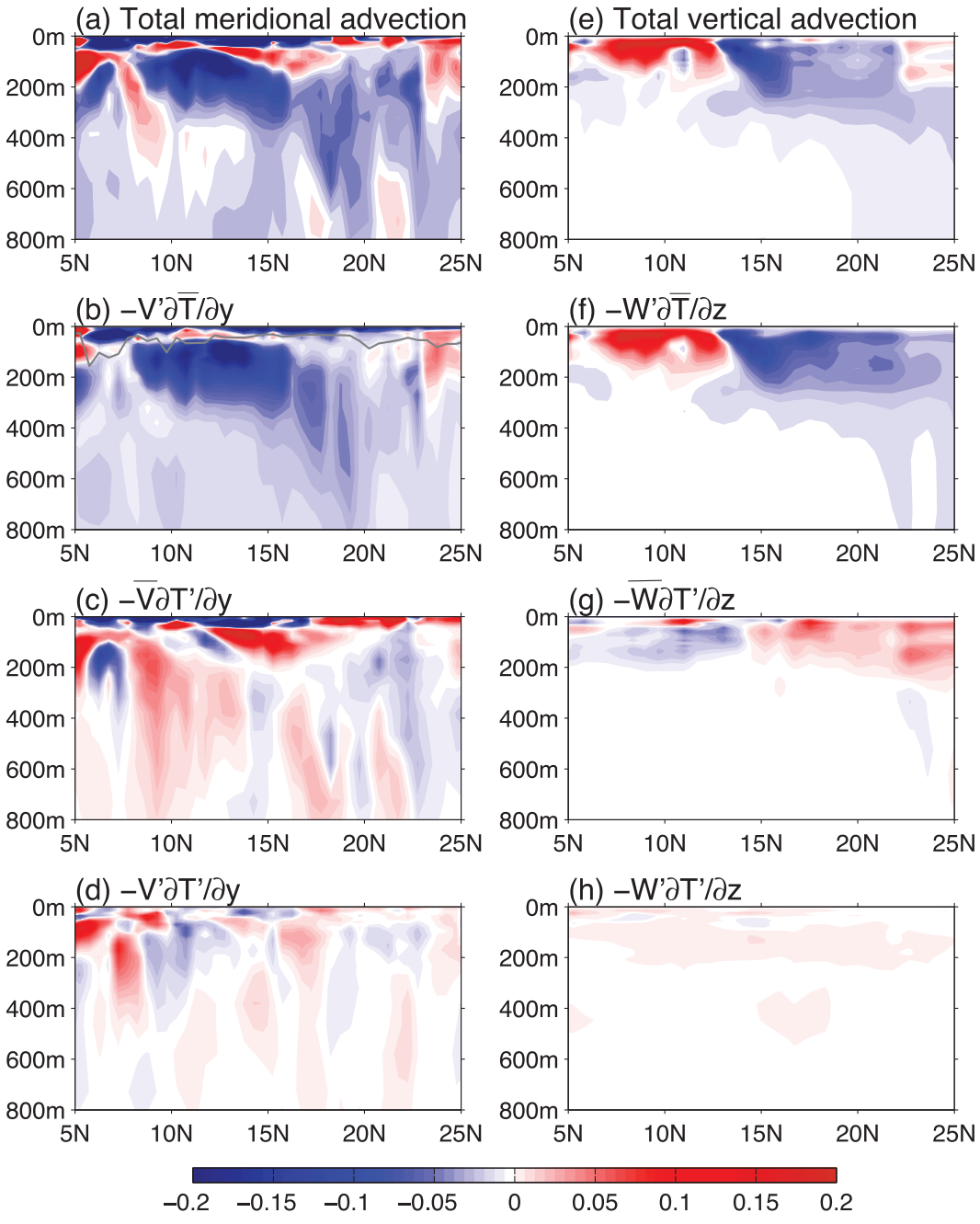

FIG. 7. Regression of advection terms (10^{-8} °C s^{-1}) onto the normalized AMO index from the SODA data. Shown are the (a) total meridional temperature advection, (b) advection by the anomalous meridional current, (c) advection by the mean meridional current, and (d) nonlinear term. (e)–(h) As in (a)–(d), but for the vertical temperature advection. The gray line in (b) denotes the mean mixed layer depth, defined by the depth where the difference with the potential density at the first layer equals 0.125 kg m^{-3}.

induced by the local process or remote forcing such as the thermocline adjustment (Zhang 2007) cannot produce the subsurface temperature cooling on multidecadal time scales. The result does not support the hypothesis by Zhang (2007), who suggested that the ocean thermocline adjustment associated with the AMOC is important for the multidecadal subsurface cooling in the TNA. In summary, the TNA subsurface cooling associated with the warm phase of the AMO is largely attributed to the advection by the anomalous northward current. North of

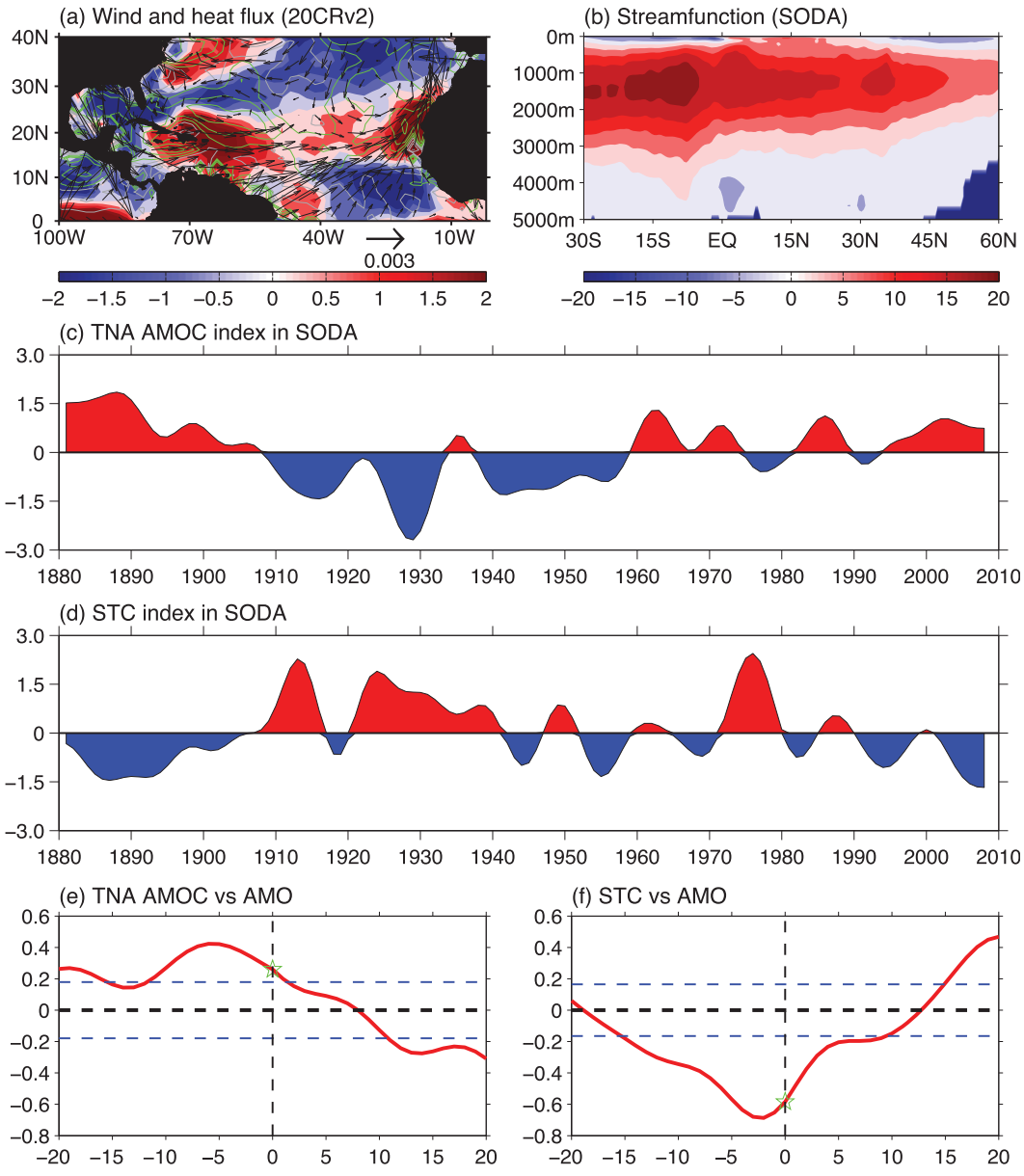

FIG. 8. (a) Regression of surface net heat flux (shading; positively downward; W m^{-2}), wind stress (vector; N m^{-2}), and wind stress curl (contour; contour interval is 1.0×10^{-9} N m^{-3}; positive and negative values are denoted by the green and gray lines, respectively) onto the normalized AMO index; (b) long-term mean AMOC streamfunction (Sv); (c) the TNA AMOC index; (d) the STC index; and lead–lag correlations of the AMO with (e) the TNA AMOC index and (f) the STC index. In (e),(f), the unit in x axis is year, and a positive (negative) year indicates the AMOC/STC leads (lags) the AMO. The horizontal dashed lines represent the 90% confidence level. The AMO and streamfunction are from the SODA data, and the heat flux and wind are from 20CRv2. The TNA AMOC index is defined as the maximum streamfunction below 300 m between 5° and 20°N, and the STC index is defined as the maximum streamfunction in the upper 250 m between 5° and 20°N.

14°N, the advection by an anomalous upwelling also contributes to the TNA subsurface cooling.

Next, we examine the TNA surface warming associated with the warm phase of the AMO. The total meridional advection shows a surface cooling in the TNA region (Fig. 7a). The surface cooling is contributed by both the advections of the anomalous and mean meridional currents ($-V'\partial\overline{T}/\partial y$ and $-\overline{V}\partial T'/\partial y$; Figs. 7b,c). Given the surface mean states (Figs. 5, 6), this indicates that there exists an anomalous surface southward current and positive SST meridional gradient anomaly. The anomalous surface southward current is largely due to the

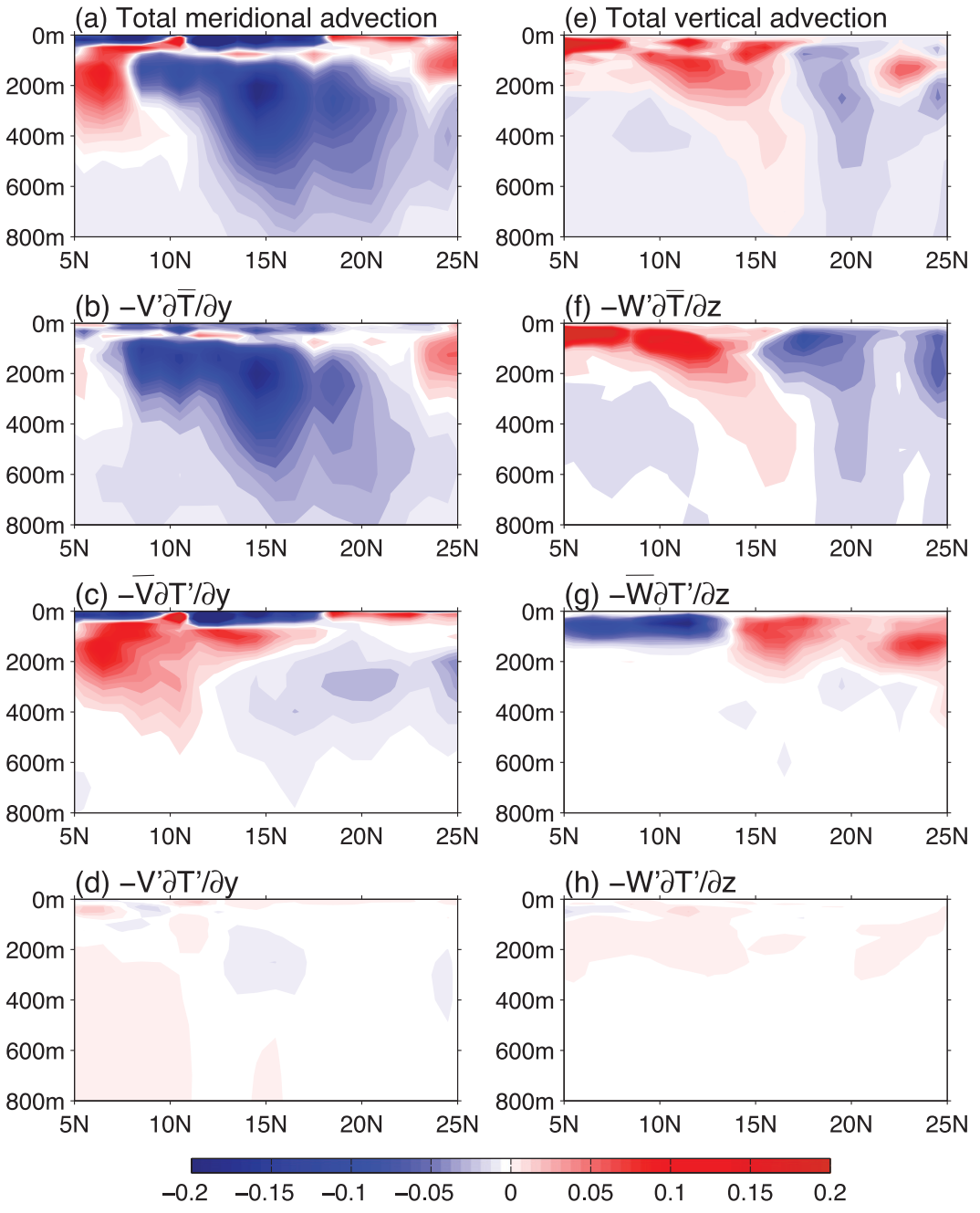

FIG. 9. Regression of advection terms (10^{-8} °C s^{-1}) onto the normalized AMO index. The regression is the ensemble mean of 12 CMIP5 models that simulate the TNA surface and subsurface temperature variation reasonably well. Shown are the (a) total meridional temperature advection, (b) advection by the anomalous meridional current, (c) advection by the mean meridional current, and (d) nonlinear term. (e)–(h) As in (a)–(d), but for the vertical temperature advection.

anomalous westerly wind–induced Ekman drift (Fig. 8a). It is also seen that there is an obvious boundary to separate the surface and subsurface cold meridional advection in Fig. 7b. This boundary approximately collocates with the ocean mixed layer and has a negligible meridional advection because of the nearly zero anomalous meridional current (the transition from the subsurface northward to surface southward flows) and temperature gradient.

The total vertical advection can explain the surface warming south of 14°N (Fig. 7e) as a result of an anomalous downwelling induced by the weakened trade

winds. However, it tends to cool the surface temperature north of 14°N because of the anomalous upwelling (Figs. 7e,f). Therefore, both the meridional and vertical advection terms cannot explain the surface warming in the TNA north of 14°N associated with the warm phase of the AMO. In fact, the surface warming in the TNA north of 14°N is primarily due to the surface net heat flux (Fig. 8a). The westerly wind anomalies associated with the warm phase of the AMO reduce the loss of turbulent heat flux and then warm the surface ocean.

c. *Physical mechanisms in CMIP5 simulations*

As shown earlier, 12 of 18 CMIP5 models simulated the out-of-phase variation of the TNA surface and subsurface ocean temperatures reasonably well. Figure 9 shows the 12-model ensemble mean of advection term regressions onto the model AMO index. Overall, the result is broadly similar to that in the SODA data. In particular, the advection by anomalous meridional current is a major contribution to the TNA subsurface ocean cooling (Fig. 9b). In comparison with the SODA data, the advection by the mean meridional current is well organized, with the TNA subsurface ocean warming and cooling south and north of 13°N, respectively (Fig. 9c). The TNA subsurface cooling north of 13°N is an obvious feature in spite of a weak magnitude. This indicates that the advection of the anomalous meridional temperature gradient by the mean meridional current can partly contribute to the subsurface cooling in the TNA, although it is not a dominant factor.

Like the result in the SODA data, the anomalous downwelling south of 14°N disfavors (favors) the TNA subsurface cooling (surface warming), whereas the opposite is true north of 14°N. In the meantime, the advection by the mean vertical velocity tends to offset but cannot overwhelm the effect of advection by the anomalous vertical velocity (Figs. 9f,g). As a result, the total vertical advection (Fig. 9e) is mainly determined by the advection because of the anomalous vertical velocity. We have to keep in mind that the contribution of the meridional advection to the TNA multidecadal temperature variation is much larger than that of the vertical advection (Fig. 9a versus Fig. 9e).

Similar to the SODA data, the model-simulated surface warming in the TNA associated with the warm phase of the AMO is also largely due to the surface net heat flux induced by the weakened trade winds (Fig. 10). Nearly all the models display a cyclonic wind stress and a weakening of the trade winds in the North Atlantic, consistent with the 20CRv2. Even in the models that do not well simulate the out-of-phase relationship between the TNA surface and subsurface ocean temperatures, the net surface flux still tends to warm the TNA surface ocean during the warm phase of the AMO (Figs. 10m–r). This suggests that the heat flux is important for the surface ocean temperature in the TNA.

In summary, the heat budget analyses from both observational data and CMIP5 models show that the anomalous northward current plays an important role in the subsurface ocean cooling (warming) in the TNA associated with the warm (cold) phase of the AMO. Given that the subsurface anomaly occurs from the mixed layer down to 800–1500 m, it is expected that the anomalous northward current may relate to both the deep AMOC and shallow STC variability. In the following sections, we will discuss the AMOC and STC relations to the TNA ocean temperature variation associated with the AMO.

5. Link of the AMO with the AMOC and STC

a. *Relation to the AMOC*

Both the SODA data and most of CMIP5 models show that, during the warm (cold) phase of the AMO, the anomalous northward (southward) meridional current is responsible for the TNA subsurface ocean cooling (warming). To examine AMOC relation to this variation, we first calculate the AMOC streamfunctions. The long-term mean streamfunctions for the SODA data and CMIP5 models are shown in Figs. 8b and 11, respectively. The mean AMOC streamfunctions show highly varying structures. The positions of the maximum overturning are typically found at 600–1500-m depth and between 20° and 60°N. There are large differences in how the models reproduce the lower overturning cell. Several models show either an absent or a very weak lower overturning cell of the Antarctic Bottom Water (AABW), while other models show the AABW all the way north to 60°N. Hydrographic observations show that the AABW almost disappears north of 35°N (Johnson 2008). CMIP5 models show a long-term mean overturning circulation range from 13 to 33 Sv ($1\ \text{Sv} \equiv 10^6\ \text{m}^3\ \text{s}^{-1}$). Based on hydrographic data, the estimates of the AMOC strength are 14–18 Sv at 24°N (Ganachaud and Wunsch 2000; Lumpkin and Speer 2003), 18.7 ± 5.6 Sv at 26.5°N (Cunningham et al. 2007), and 13–19 Sv at 48°N (Ganachaud 2003). Generally speaking, CMIP5 models basically capture the feature of the AMOC although the magnitude and location are a little bit different from observations.

The AMOC index in the TNA is defined as the maximum streamfunction in the latitude band of 5°–20°N. Similar results can be obtained if we choose a specific latitude in the TNA (not shown). To reduce and/or exclude the surface wind driven overturning, we have used

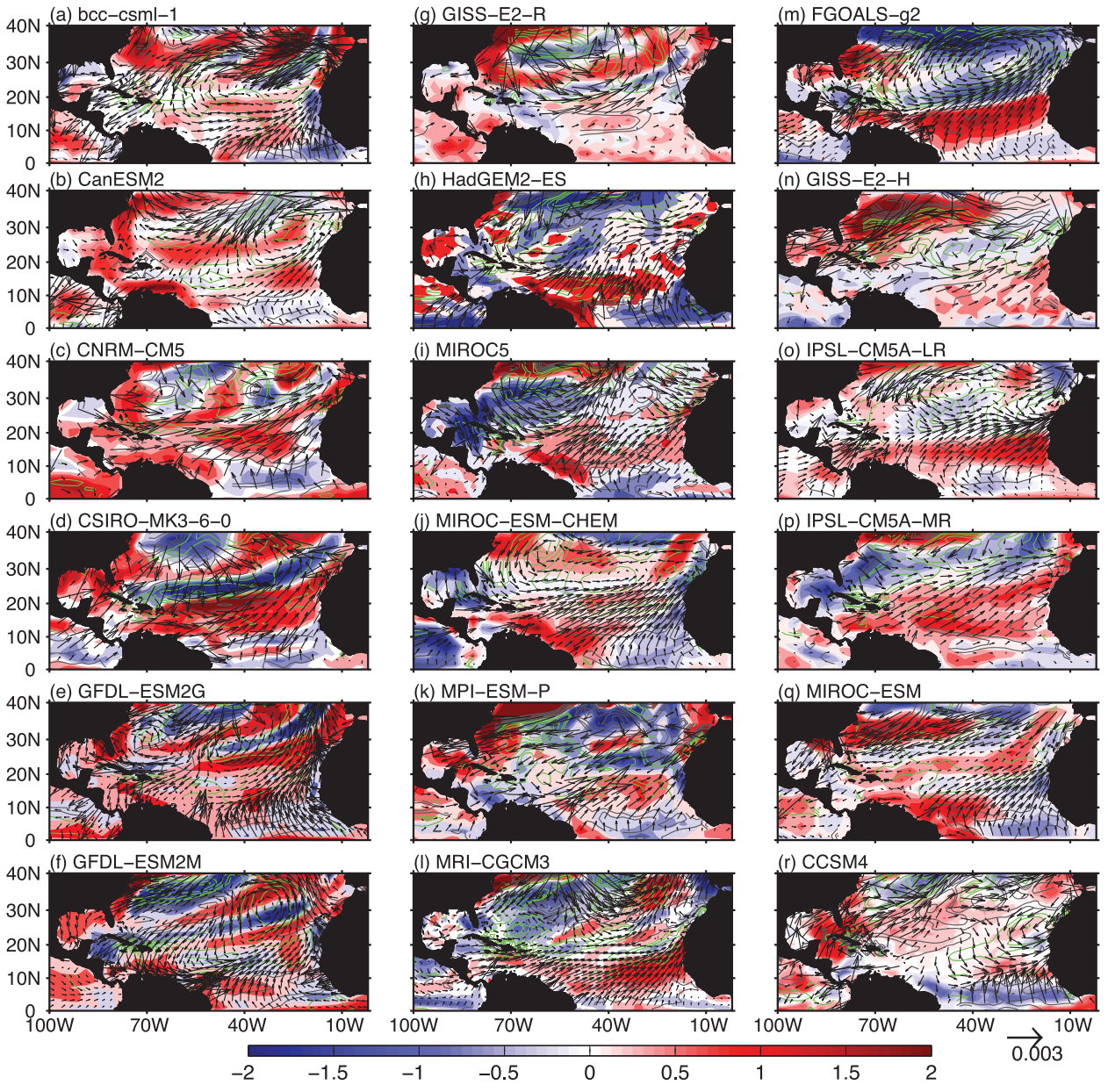

FIG. 10. Regression of surface net heat flux (shading; positively downward; $W\,m^{-2}$), wind stress (vector; $N\,m^{-2}$), and wind stress curl (contour; contour interval is $1.0 \times 10^{-9}\,N\,m^{-3}$; positive and negative values are denoted by the green and gray lines, respectively) onto the corresponding normalized AMO index in CMIP5 models.

a further criterion that the maximum should be located deeper than 300 m. The AMOC indices in the TNA for the SODA data and CMIP5 models are shown in Figs. 8c and 12. To emphasize the multidecadal variability, we have detrended and smoothed the indices by a 7-yr low-frequency filter. An initial impression is that these TNA AMOC indices vary differently. However, a close examination finds that the TNA AMOC indices in the SODA data and most of CMIP5 models vary with their individual AMO indices. The feature can be clearly seen from the correlation plots in Figs. 8e and 13. At the zero time lag, the TNA AMOC and AMO indices are positively correlated in the SODA data and the 12 CMIP5 models that are able to simulate the TNA subsurface ocean cooling (Figs. 8e, 13a–l). For the six models that are unable to simulate the subsurface ocean cooling, the correlations are negative except the nearly zero correlation of IPSL-CM5A-MR (Figs. 13m–r). This implies that the TNA AMOC is strengthened (weakened) during the warm (cold) phase of the AMO. It

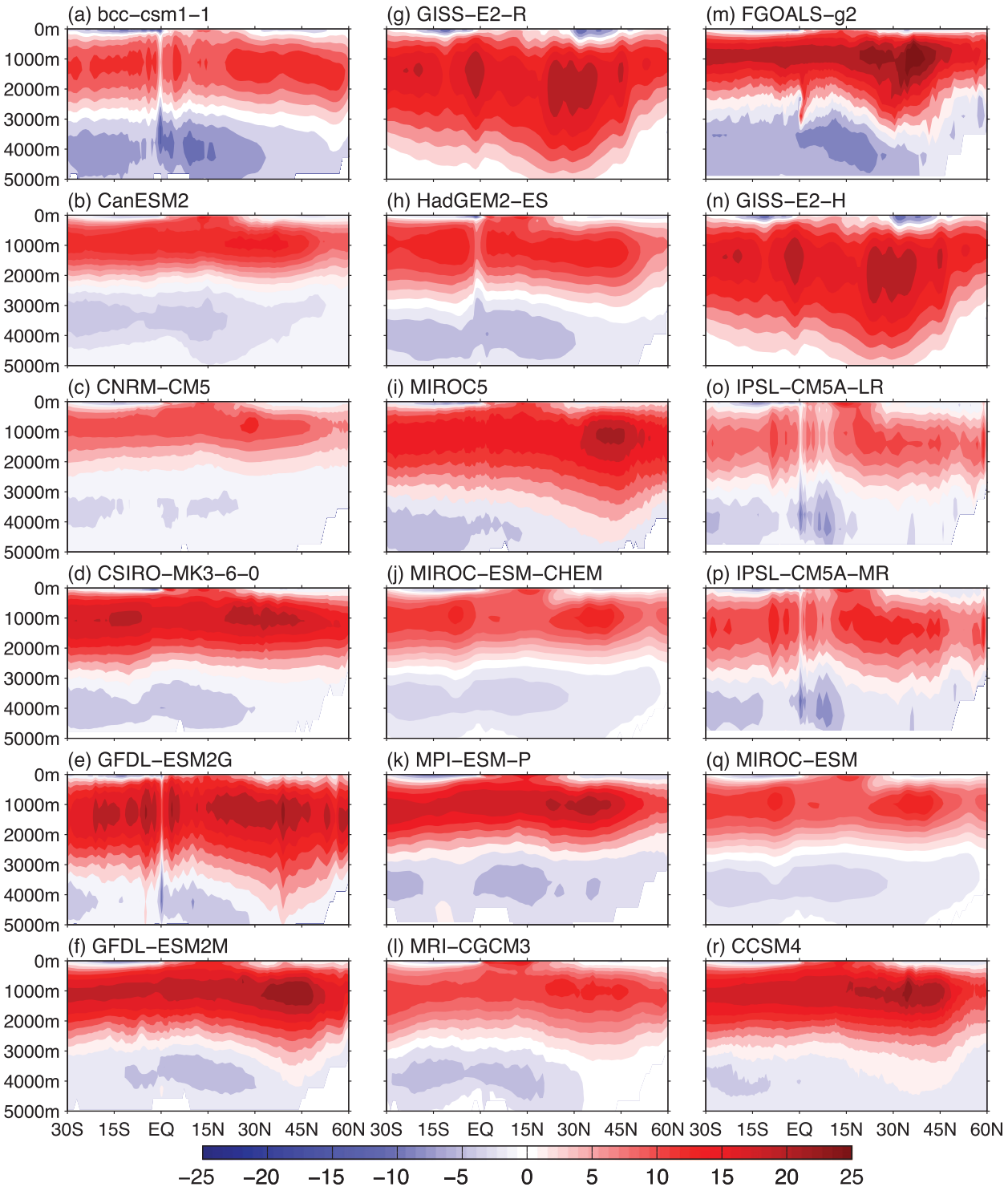

FIG. 11. Long-term mean AMOC streamfunction (Sv) from CMIP5 models.

also means that there is an anomalous northward (southward) current in the TNA upper-ocean layer during the warm (cold) phase of the AMO, which in turn induces the TNA subsurface cooling (warming). This is consistent with the result of the heat budget analysis shown earlier for the SODA data and the 12 models showing realistic subsurface temperature anomalies.

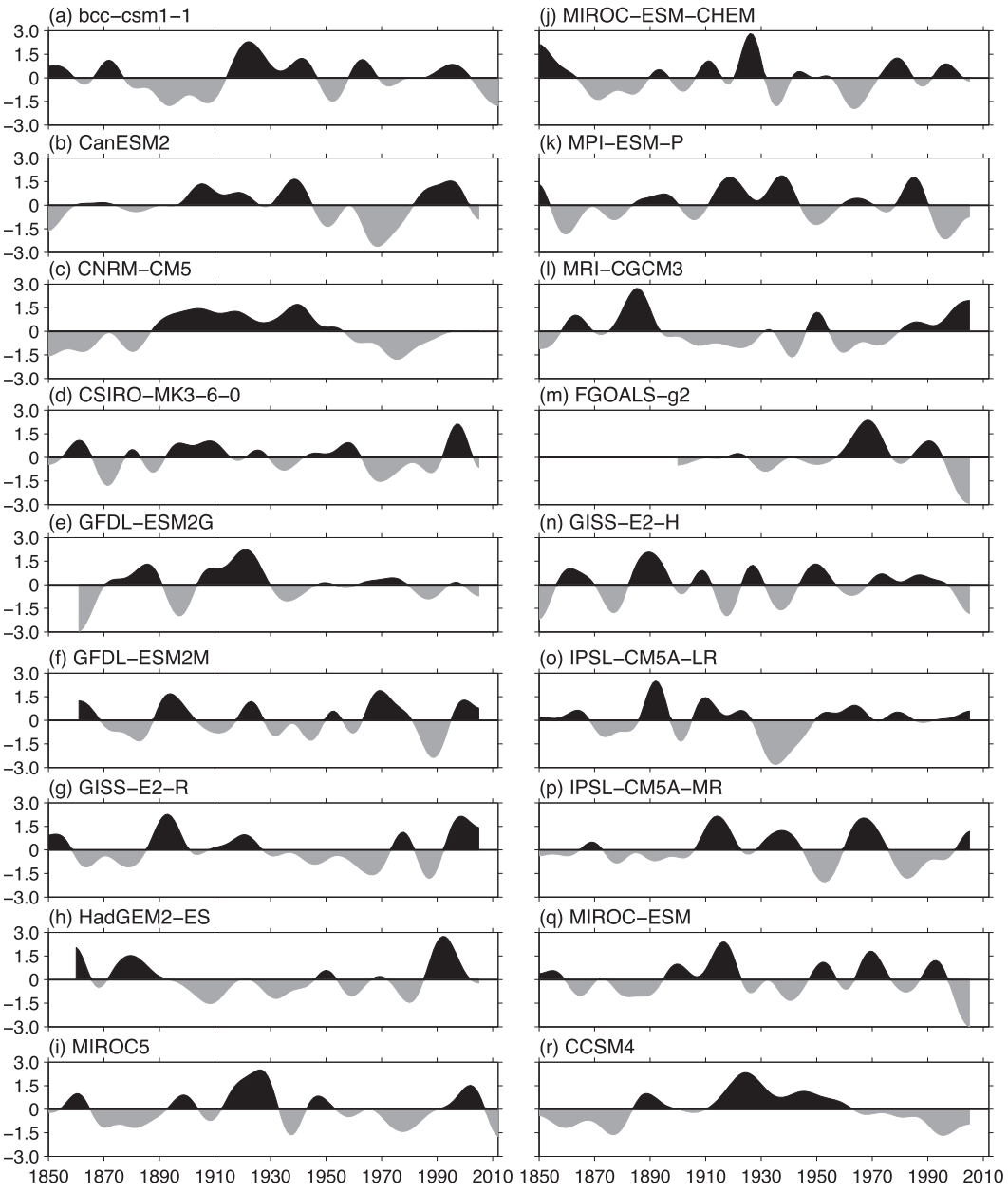

FIG. 12. The TNA AMOC index defined as the maximum streamfunction below 300 m from 5° to 20°N from CMIP5 models. All time series are normalized by their standard deviation.

Previous studies suggested that the AMOC variations have a latitudinal dependence (Mignot and Frankignoul 2005; Msadek and Frankignoul 2009; Zhang 2010). These studies showed that the subpolar AMOC variation leads the subtropical and tropical AMOC variations by several years (about 5 yr in GFDL CM2.1) and the length of time lag is mainly determined by the advection speed in the North Atlantic deep-water formation region (Zhang 2010). Here, we also analyze the high–low latitudinal dependence of the relationship between the AMOC and AMO in CMIP5 simulations. In the higher latitudes, most of the models show that the AMOC leads the AMO (not shown). As the latitude decreases, the leading time becomes smaller and the relationship between the AMOC and AMO becomes more and more synchronized. Thus, the warm (cold) phase of the AMO corresponds to a strengthened (weakened) TNA AMOC in the nearly zero time lag.

The positive correlations between the AMO and TNA AMOC in the SODA data and CMIP5 models maximize

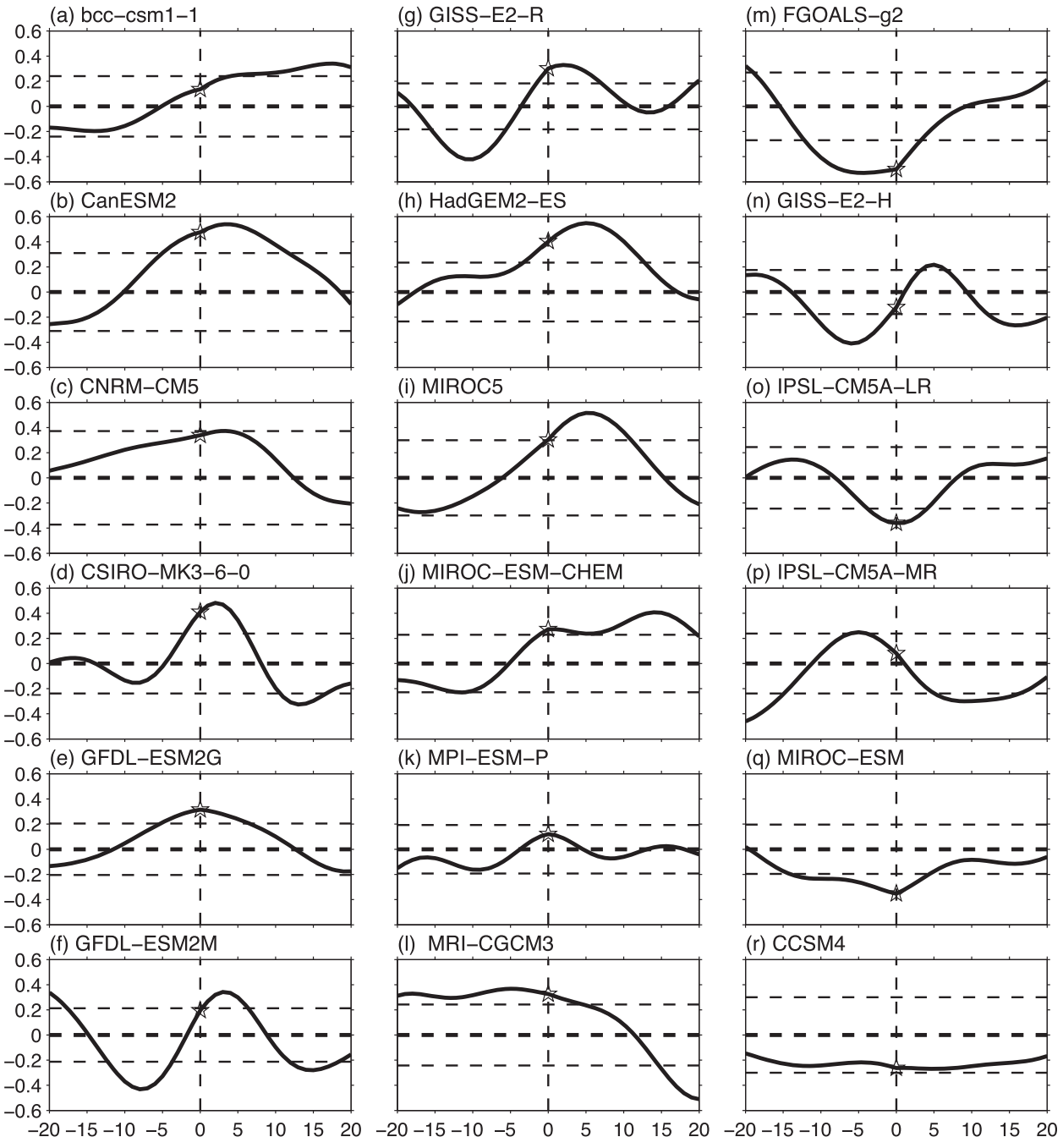

FIG. 13. Lead–lag correlations between the AMO and TNA AMOC index from CMIP5 models. The unit in *x* axis is year. Positive (negative) year in *x* axis means the AMOC leads (lags) the AMO. The horizontal dashed line indicates the 90% confidence level.

in different ways. Some models show zero time lag (e.g., GFDL-ESM2G). Some models show that the maximum correlation occurs when the TNA AMOC leads by several years (e.g., GFDL-ESM2M), while the correlation in the SODA data maximizes when the AMO leads the TNA AMOC by 5 yr (Fig. 8e). This inconsistency may arise from the different adjustment time of the TNA AMOC (determined by the advection speed) to northern Atlantic deep convection. The other possibility may be from external factors' interference such as aerosols.

b. Relation to the STC

The Atlantic STC is a shallow overturning cell connecting the subtropics with the equatorial region of the

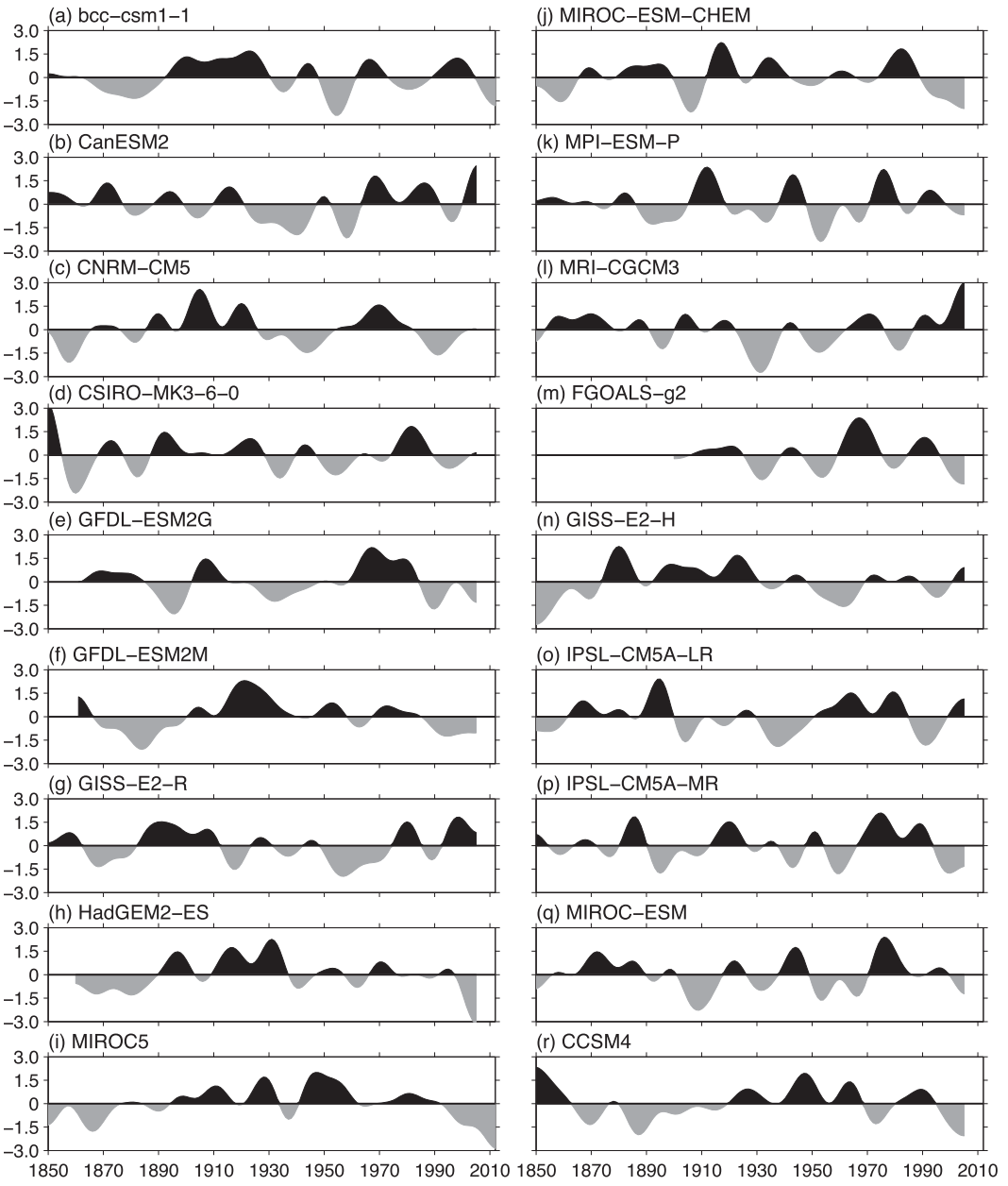

FIG. 14. The Atlantic STC index defined as the maximum streamfunction in the upper 250 m between 5° and 20°N from CMIP5 models. All time series are normalized by their standard deviation.

Atlantic Ocean (e.g., Malanotte-Rizzoli et al. 2000; Zhang et al. 2003). Water mass that is subducted into the thermocline in the eastern subtropics of both hemispheres is swept westward by the north and south equatorial currents, respectively. The water mass eventually reaches to the equatorial undercurrent, drifts eastward and upwells in the eastern equator. In conjunction with the surface northward Ekman current, it forms a shallow (mainly in the upper ocean of 250 m) overturning cell: that is, the Atlantic STC. To obtain the Atlantic STC variability in the Northern Hemisphere, we choose two methods to define the STC index. One is similar to the Pacific STC (McPhaden and Zhang 2002, 2004; Schott et al. 2007, 2008), which chooses the coast-to-coast transport across 9°N as an STC index. The other definition is similar to the AMOC index, which is defined as the maximum streamfunction in the latitude band of 5°–20°N in the upper 200 m. Although there are some magnitude differences in the two definitions, the phase variability is very similar. So we only show results

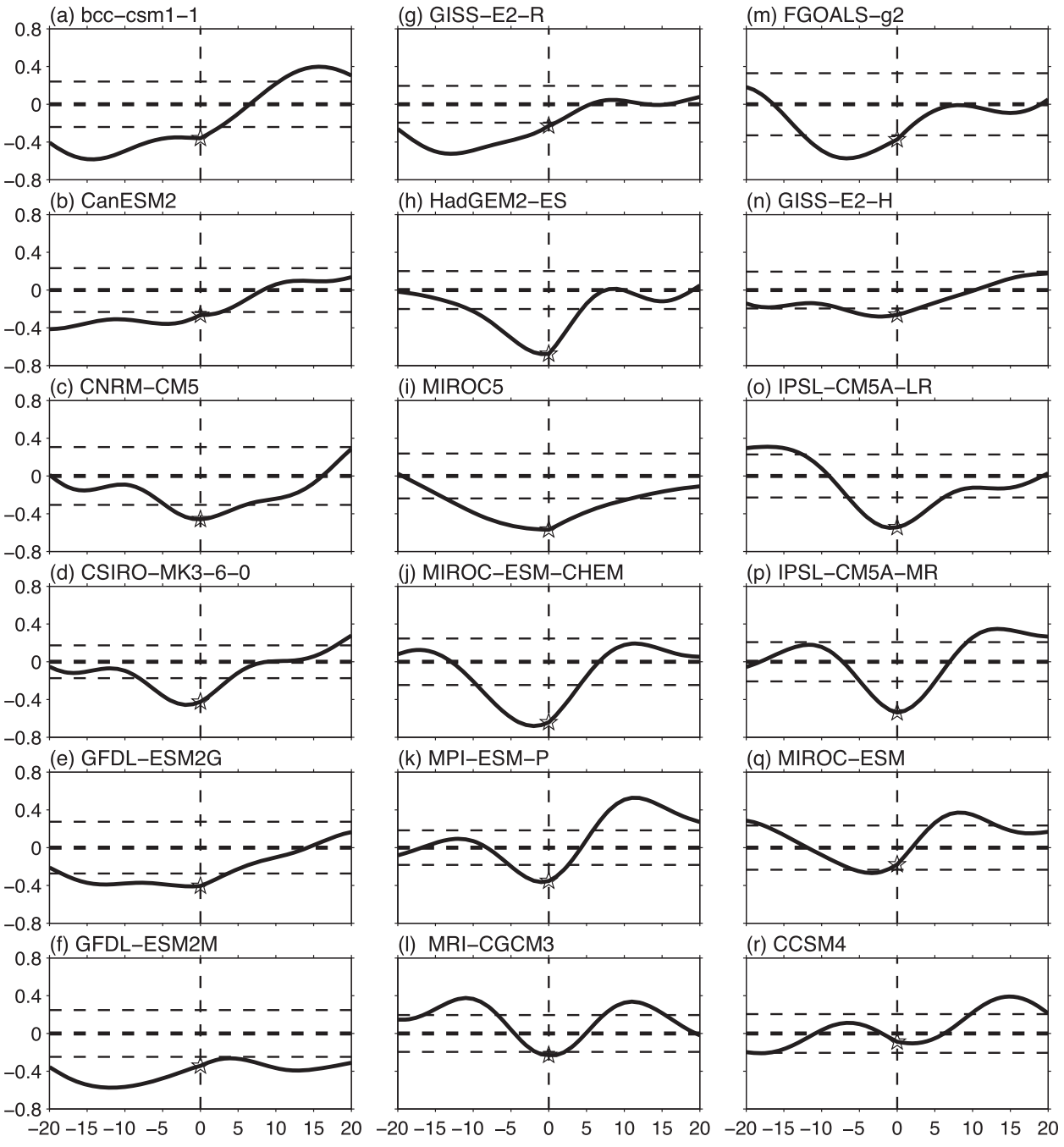

FIG. 15. Lead–lag correlations between the AMO and STC index from CMIP5 models. The unit in the *x* axis is years. A positive (negative) year in the *x* axis means the STC leads (lags) the AMO. The horizontal dashed line indicates the 90% confidence level.

from the second definition in this paper. Similar results can be obtained by using the first definition, in particular for the normalized STC index and correlations with the AMO index.

The Atlantic STC indices in the SODA data and CMIP5 models are displayed in Figs. 8d and 14. The multidecadal STC variability is different from the TNA AMOC variability (Fig. 8c versus Fig. 8d and Fig. 12 versus Fig. 14). For the SODA data and 12 CMIP5 models that are able to simulate the out-of-phase relationship between the TNA surface and subsurface temperatures, the STC indices are negatively correlated with the TNA AMOC indices at the zero time lag, whereas for the other 6 models the correlations are

either positive or nearly zero (not shown). Since we are interested in examining the contribution of the meridional current to the TNA subsurface temperature variation associated with the AMO, we focus on the lead–lag correlations between the AMO and STC indices. All the models and SODA data show a negative correlation between the AMO and STC indices with a zero time lag (Figs. 8f, 15). This indicates that the northern Atlantic STC is significantly weakened (strengthened) during the warm (cold) phase of the AMO. The weakening (strengthening) of the STC is accompanied by an anomalous northward (southward) current in the subsurface (about 100–200 m) and an anomalous southward (northward) Ekman drift in the surface. The anomalous subsurface northward current associated with the AMO produces the multidecadal subsurface cooling as exhibited in Figs. 1b,f and 4, at least in the upper 200 m. Of course, the weakening of the STC cannot induce the cooling anomaly in the ocean deep layer (because of its shallow feature) which is due to the AMOC variation as discussed in last subsection.

The STC variation associated with the AMO can be explained by the surface wind variation, particularly the trade winds and the associated subtropical wind stress curl (Figs. 8a, 10). The weakening (strengthening) of the surface trade winds and a positive (negative) subtropical wind stress curl anomaly correspond to a decrease (an increase) of the STC. This is because the interior southward transport, which is a key element of the subsurface branch of the STC, is primarily determined by the subtropical wind stress curl. Meanwhile, the surface northward Ekman transport (the upper branch of the STC) is mainly determined by the strength of the trade winds. Because all models and observational data show a weakening (strengthening) of the trade winds and a positive (negative) subtropical wind stress curl during the warm (cold) phase of the AMO, the Atlantic STC is all weakened (strengthened) as shown in Figs. 15 and 8f.

c. *Interpreting subsurface cooling by the enhanced AMOC and weakened STC*

As shown in previous sections, the warm (cold) phase of the AMO is accompanied by the subsurface ocean cooling (warming) in the TNA that is mainly attributed to the meridional advection by an anomalous northward (southward) in the subsurface ocean. Our analyses have further shown that the warm (cold) phase of the AMO is associated with a strengthening (weakening) of the TNA AMOC in the SODA data and 12 CMIP5 models, but the opposite is true for the other 6 CMIP5 models. The SODA data and these 12 models do show the TNA subsurface ocean cooling (warming) during the warm (cold) phase of the AMO, whereas these 6 models do not well simulate the subsurface cooling (warming). However, all 18 models and the SODA data show that the warm (cold) phase of the AMO corresponds to a weakening (strengthening) of the Atlantic STC. The strengthening (weakening) of the AMOC features an anomalous northward (southward) current in the TNA subsurface ocean, and so does the weakening (strengthening) of the STC. These suggest that both the variations of the AMOC and STC can contribute to the subsurface ocean cooling (warming), but the AMOC contribution seems to be more important.

We first consider the case for the SODA data and the 12 CMIP5 models that are able to simulate the out-of-phase variation between the TNA surface and subsurface ocean temperatures. If the ocean mixing in the deep-water formation region increases, the associated high latitude AMOC strengthens (e.g., Stocker et al. 2007; Zhang et al. 2011). Then, the AMOC signal propagates southward accompanied with the advection, coastal and equatorial Kelvin waves, and Rossby waves (e.g., Zhang 2010). After several years later, the AMOC in the TNA reaches to the maximum; induces an anomalous northward current in the upper 1500 m; and thus generates a TNA subsurface ocean cooling between 8° and 20°N, where the mean meridional temperature gradient is positive because of the 9°N temperature dome. Meanwhile, at the surface the strengthened AMOC leads to a substantial North Atlantic and TNA surface warming (the warm phase of the AMO) as a result of the increased net heat flux and increased northward heat transport. The TNA surface warming decreases the surface pressure, induces an anomalous surface convergence, and thus generates a weakening of the trade winds and a positive wind stress curl anomaly in the subtropical North Atlantic. On one hand, the weakened trade winds tend to warm SST by decreasing the turbulent heat flux loss and increasing the Ekman drift–induced downwelling. On the other hand, the weakened trade winds and positive wind stress curl anomaly reduce the shallow STC strength and the associated subsurface southward interior current, generating an anomalous northward current. Thus, like the AMOC, the STC also acts to cool the TNA subsurface ocean.

The situation is different for the six CMIP5 models that are not well simulate the out-of-phase variation between the TNA surface and subsurface ocean temperatures. These models show that the warm (cold) phase of the AMO is associated with a weakening (strengthening) of the AMOC in the TNA. So the models cannot simulate the anomalous northward (southward) current induced by the AMOC in the TNA subsurface ocean that is required for the subsurface cooling (warming) during the

warm (cold) phase of the AMO. However, these six models are able to simulate the inverse relationship between the shallow STC and AMO because the STC is mostly wind driven (the models do simulate the feature of the weakened trade winds). This means that the simulated warm (cold) phase of the AMO is associated with a weakening (strengthening) of the STC. The weakening (strengthening) of the STC induces an anomalous northward (southward) current, which can make a contribution to the subsurface ocean cooling (warming) in the TNA. However, this contribution is not large enough for the models to fully simulate the out-of-phase variation between the subsurface and surface ocean temperatures in the TNA.

6. Multidecadal salinity variation in the TNA

Given the feature of the TNA surface and subsurface temperature variation, a natural question is: Does salinity show a similar variation in the TNA? Using the pentadal salinity data of the *World Ocean Database 2005* (Boyer et al. 2006), Wang et al. (2010) showed that the salinity anomalies do not seem to display an out-of-phase relationship between the surface and subsurface oceans in the TNA associated with the AMO (see their Fig. 10). Here we also calculate the regressions of the Atlantic zonal mean ocean salinity onto the AMO index for the SODA and Ishii data (Figs. 16s,t). The SODA regression is similar to the result of Wang et al. (2010), which shows a uniform freshening in the TNA surface and subsurface oceans. The Ishii salinity regression does not seem to show an obvious out-of-phase relation either, although there is a positive salinity regression near the surface north of 15°N (Fig. 16t). We have to keep in mind that the salinity data may not be reliable, especially during earlier times.

The regressions of the Atlantic zonal mean ocean salinity onto their individual AMO indices for the 18 CMIP5 models are shown in Figs. 16a–r. For most of the 12 models that are able to simulate the multidecadal TNA temperature variation, they also produce the out-of-phase relation in the TNA surface and subsurface ocean salinity (Figs. 16a–l). During the warm (cold) phase of the AMO, these models show the negative salinity anomalies in the TNA subsurface ocean and the positive salinity anomalies in the surface ocean. For the six models that are unable to simulate the out-of-phase temperature variation, they cannot well produce the negative salinity anomalies in the TNA subsurface ocean either (Figs. 16m–r).

We also calculate the salinity variation contribution by the ocean advection terms. The salinity variation is largely determined by the meridional salinity advection. The 12-model ensemble mean of the regressions of the meridional salinity advection terms onto the AMO index is shown in Fig. 17. It is shown that the total meridional advection can explain the decreased salinity in the TNA subsurface ocean and the increased salinity in the TNA surface ocean (Fig. 17a). A further decomposition shows that the salinity advection by the anomalous meridional current plays a dominant role and the other terms are secondary (Figs. 17b–d). Given the positive mean meridional salinity gradient ($\partial\overline{S}/\partial y > 0$), Fig. 17b indicates that the TNA subsurface ocean has an anomalous northward current, whereas the surface ocean flow is anomalously southward. These are consistent with the results in the last section that these 12 models are associated with a strengthening of the TNA AMOC and a weakening of the Atlantic STC during the warm phase of the AMO, which both result in an anomalous northward current in the subsurface ocean. The surface anomalous southward flow is due to the Ekman transport induced by the weakened trade winds associated with the warm phase of the AMO. Thus, the model-simulated AMOC and STC can also contribute to the salinity variation of the TNA subsurface and surface oceans on multidecadal time scales.

7. Discussion and conclusions

The paper uses observational data and CMIP5 model simulations to show and examine the variations of the Atlantic multidecadal oscillation (AMO), Atlantic meridional overturning circulation (AMOC), subtropical cell (STC), and surface wind in the North Atlantic. It is shown that the tropical North Atlantic (TNA) features an anticorrelated variation in the surface and subsurface ocean temperatures associated with the AMO. That is, the warm (cold) phase of the AMO is accompanied by a warm (cold) surface ocean and a cold (warm) subsurface ocean in the TNA. Given that there is no significant rapid TNA subsurface response to changes in the radiative forcing, this multidecadal TNA subsurface temperature anomaly can be taken as a proxy or fingerprint for the AMOC variation (Zhang 2007). Here we show that the anticorrelated surface and subsurface temperature variation in the TNA does indeed link with the variations of both the AMOC and STC. We found that the TNA subsurface temperature variation is largely attributed to the advection by the anomalous meridional current ($-V'\partial\overline{T}/\partial y$), which is induced by the AMOC and STC variations. Because the mean meridional temperature gradient in the TNA subsurface is positive ($\partial\overline{T}/\partial y > 0$) because of the temperature dome at 9°N, the anomalous subsurface current induced by the AMOC and STC basically controls the variation of the TNA subsurface temperature. The advections of the

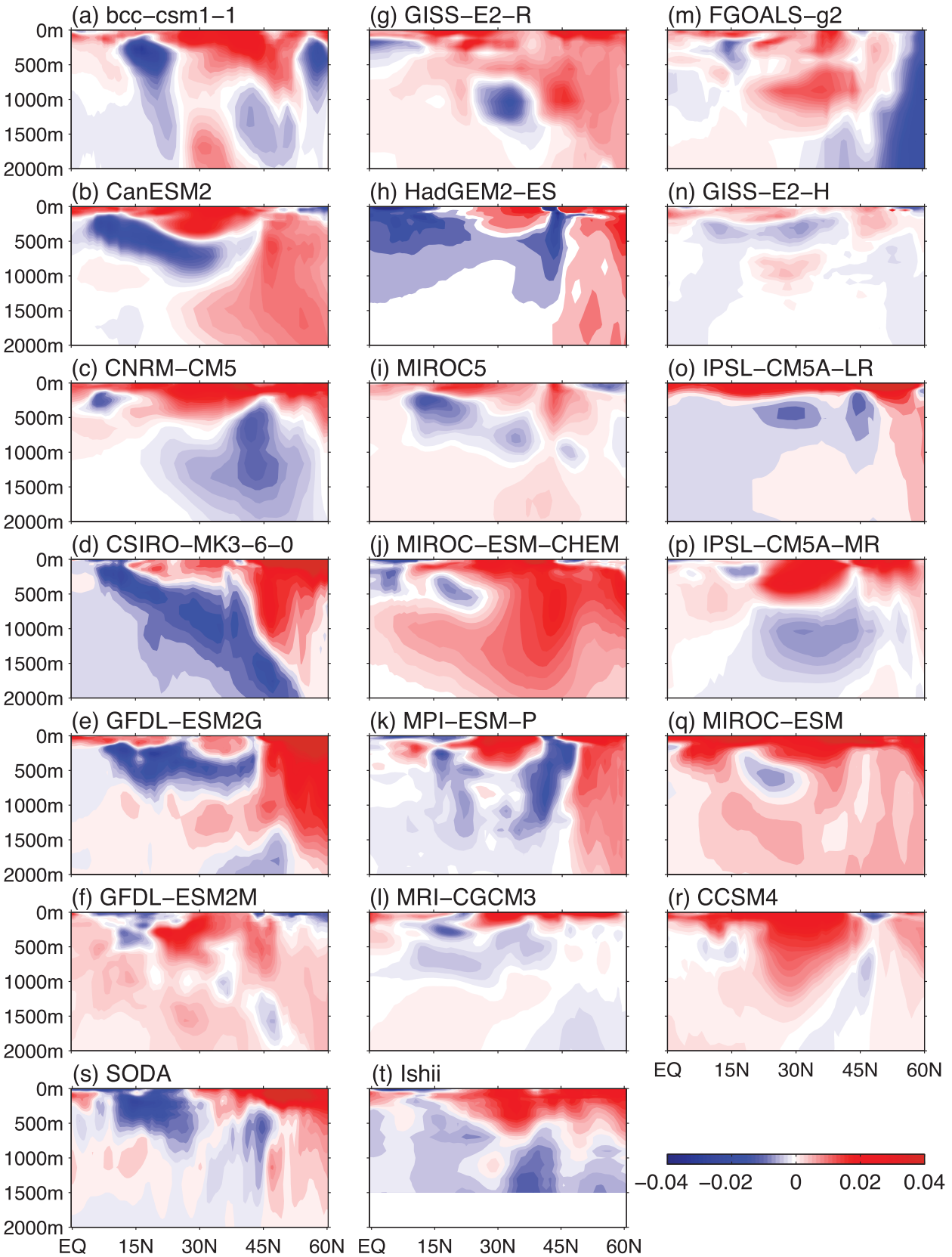

FIG. 16. Regression of the Atlantic zonal mean salinity (psu) onto the normalized AMO index from (a)–(r) CMIP5 models, (s) SODA data, and (t) Ishii data.

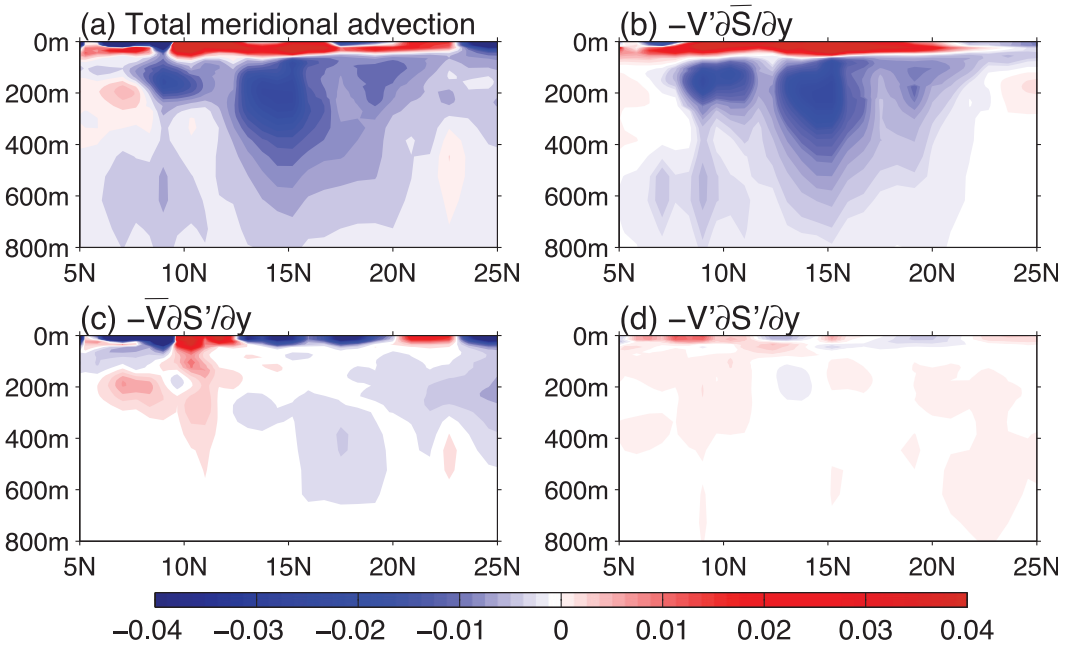

FIG. 17. Regression of salinity advection terms (10^{-8} psu s^{-1}) onto the normalized AMO index. The regression is the ensemble mean of 12 CMIP5 models that simulate the TNA surface and subsurface temperature variation reasonably well. Shown are the (a) total meridional salinity advection, (b) advection by the anomalous meridional current, (c) advection by the mean meridional current, and (d) nonlinear term.

anomalous temperature gradients by the mean currents ($-\overline{W}\partial T'/\partial z$ and $-\overline{V}\partial T'/\partial y$) are of secondary importance in controlling the TNA subsurface temperature variation. This suggests that the temperature gradient changes induced by the local process or remote forcing such as the thermocline adjustment (Zhang 2007) cannot produce the subsurface temperature cooling associated with the warm phase of the AMO.

The variations of the AMOC, STC, ocean temperature, and surface wind with the AMO can be summarized in Fig. 18. A strengthening of the AMOC is associated with the AMOC anomaly signal in the high

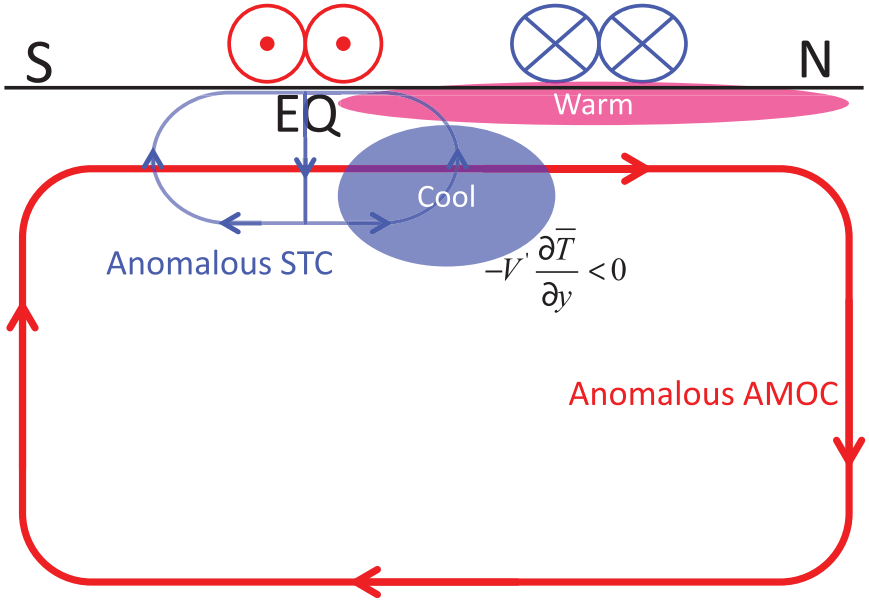

FIG. 18. Schematic diagram showing the variations of the AMOC, STC, ocean temperature, and surface wind with the AMO on multidecadal time scales.

latitude that propagates southward, which is accompanied with the advection, coastal and equator Kelvin waves, and Rossby waves (e.g., Zhang 2007). Several years later, the strength of the TNA AMOC reaches to its maximum, which induces an anomalous northward current in the upper ocean of 2000 m and thus generates a TNA subsurface cooling between 8° and 20°N where the mean meridional temperature gradient is positive because of the 9°N temperature dome. Meanwhile, in the surface, the strengthened AMOC leads to a substantial North Atlantic and TNA surface warming (i.e., the warming during the warm phase of the AMO). The TNA surface warming decreases the surface pressure, induces an anomalous surface convergence, and thus generates a weakening of the trade winds and a positive wind stress curl anomaly over the subtropical North Atlantic. On one hand, the weakened trade winds tend to warm the surface ocean by decreasing the turbulent heat flux loss and increasing the Ekman drift–induced downwelling. On the other hand, the weakened trade winds and positive wind stress curl anomaly weaken the STC and the associated subsurface southward interior current, generating an anomalous northward current and thus a subsurface cooling in the TNA. The opposite is true for a weakening of the AMOC.

The mechanism is operated in the SODA data and 12 CMIP5 model simulations. In the SODA data and 12 CMIP5 models, the warm (cold) phase of the AMO is associated with a strengthening (weakening) of the TNA AMOC and a weakening (strengthening) of the STC, which both induce an anomalous northward (southward) subsurface current and thus cool (warm) the TNA subsurface ocean. However, six CMIP5 models cannot simulate the anomalous northward (southward) current induced by the AMOC in the TNA subsurface ocean during the warm (cold) phase of the AMO. However, these six models are able to produce a weakening (strengthening) of the STC associated with the warm (cold) phase of the AMO because the STC is mostly wind driven (these models do simulate the feature of the weakened trade winds). The weakening (strengthening) of the STC does induce an anomalous northward (southward) current which can make a contribution to the subsurface ocean cooling (warming) in the TNA. However, this contribution is not large enough for these six models to fully simulate the out-of-phase variation between the subsurface and surface ocean temperatures in the TNA. This suggests that the AMOC plays a more important role than the STC in the anticorrelated variation of the TNA surface and subsurface ocean temperatures. In other words, a positive correlation between the TNA AMOC and the AMO is required for models to simulate the anomalous meridional current in the TNA subsurface ocean and then to change the subsurface ocean temperature.

For most of the 12 CMIP5 models that are able to simulate the multidecadal TNA temperature variation, they also produce an out-of-phase relation in the TNA surface and subsurface ocean salinity. During the warm (cold) phase of the AMO, these models show the negative salinity anomalies in the TNA subsurface ocean and the positive salinity anomalies in the surface ocean. The mechanism is similar to that of the temperature variation. In these models, the ocean salinity variations in the TNA are largely determined by the meridional advection associated with the AMOC and STC variations.

The present paper shows that an anomalous meridional current in the TNA subsurface ocean is required for simulating the subsurface ocean temperature and salinity variations associated with the AMO. Both the AMOC and STC can contribute to the subsurface meridional current. However, a quantitative separation of the meridional flows induced by the AMOC and STC is difficult by analyzing the data and model outputs only. Numerical model experiments are needed for addressing this issue. For example, two parallel model runs can be conducted. The first run is a fully coupled model experiment. The second run is the same as the first one but with a wind prescribing to the climatological wind in the TNA region. In this case, the STC cannot be changed by the wind variation. By comparing these two model experiments, we can obtain the relative contribution of the AMOC and STC to the anomalous meridional current in the subsurface ocean. Assessing the quantitative effect of the AMOC and STC remains challenge and is beyond the scope of this paper.

The variations of the ocean temperature in the TNA region are very important because they directly affect hurricane activity in the North Atlantic (e.g., Shay et al. 2000). However, almost all of previous studies on long-term hurricane variations use the SST variations only (e.g., Goldenberg et al. 2001; Wang et al. 2008). The present paper and others (Zhang 2007; Wang et al. 2010) show that on multidecadal time scales the TNA surface and subsurface ocean temperatures vary differently. In other words, the multidecadal temperature variations in the TNA are different if we use different upper-ocean layers (see Figs. 1, 2). Thus, a caution should be exercised for interpreting hurricane activity in terms of the multidecadal ocean temperature variation in the TNA.

Acknowledgments. We thank three anonymous reviewers and the editor John Chiang for their comments on the manuscript. This work was supported by grants from National Oceanic and Atmospheric Administration (NOAA)/Climate Program Office and the base funding

of NOAA/Atlantic Oceanographic and Meteorological Laboratory (AOML). The findings and conclusions in this report are those of the author(s) and do not necessarily represent the views of the funding agency.

REFERENCES

Booth, B. B. B., N. J. Dunstone, P. R. Halloran, T. Andrews, and N. Bellouin, 2012: Aerosols implicated as a prime driver of twentieth-century North Atlantic climate variability. *Nature,* **484,** 228–232.

Boyer, T. P., and Coauthors, 2006: *World Ocean Database 2005.* NOAA Atlas NESDIS 60, 190 pp.

Carton, J. A., and B. S. Giese, 2008: A reanalysis of ocean climate using Simple Ocean Data Assimilation (SODA). *Mon. Wea. Rev.,* **136,** 2999–3017.

Compo, G. P., and Coauthors, 2011: The Twentieth Century Reanalysis Project. *Quart. J. Roy. Meteor. Soc.,* **137,** 1–28.

Corre, L., L. Terray, M. Balmaseda, A. Ribes, and A. Weaver, 2012: Can oceanic reanalyses be used to assess recent anthropogenic changes and low-frequency internal variability of upper ocean temperature? *Climate Dyn.,* **38,** 877–896.

Cunningham, S. A., and Coauthors, 2007: Temporal variability for the Atlantic meridional overturning circulation at 26.5°N. *Science,* **317,** 935–937, doi:10.1126/science.1141304.

Delworth, T. L., and M. E. Mann, 2000: Observed and simulated multidecadal variability in the Northern Hemisphere. *Climate Dyn.,* **16,** 661–676.

Enfield, D. B., A. M. Mestas-Nuñez, and P. J. Trimble, 2001: The Atlantic multidecadal oscillation and its relation to rainfall and river flows in the continental U.S. *Geophys. Res. Lett.,* **28,** 2077–2080.

Folland, C. K., D. E. Parker, and T. N. Palmer, 1986: Sahel rainfall and worldwide sea temperatures, 1901–85. *Nature,* **320,** 602–607.

——, A. W. Colman, D. P. Rowell, and M. K. Davey, 2001: Predictability of northeast Brazil rainfall and real-time forecast skill, 1987–98. *J. Climate,* **14,** 1937–1958.

Ganachaud, A., 2003: Large-scale mass transports, water mass formation, and diffusivities estimated from World Ocean Circulation Experiment (WOCE) hydrographic data. *J. Geophys. Res.,* **108,** 3213, doi:10.1029/2002JC001565.

——, and C. Wunsch, 2000: Improved estimates of global ocean circulation, heat transport and mixing from hydrographic data. *Nature,* **408,** 453–457.

Goldenberg, S. B., C. W. Landsea, A. M. Mestas-Nuñez, and W. M. Gray, 2001: The recent increase in Atlantic hurricane activity: Causes and implications. *Science,* **293,** 474–479.

Gray, W. M., J. D. Sheaffer, and C. W. Landsea, 1997: Climate trends associated with multidecadal variability of Atlantic hurricane activity. *Hurricanes: Climate and Socioeconomic Impacts,* H. F. Diaz and R. S. Pulwarty, Eds., Springer, 15–53.

Hansen, J., and Coauthors, 2005: Earth's energy imbalance: Confirmation and implications. *Science,* **308,** 1431–1435.

Ishii, M., M. Kimoto, K. Sakamoto, and S. I. Iwasaki, 2006: Steric sea level changes estimated from historical ocean subsurface temperature and salinity analyses. *J. Oceanogr.,* **62,** 155–170.

Johnson, G. C., 2008: Quantifying Antarctic Bottom Water and North Atlantic Deep Water volumes. *J. Geophys. Res.,* **113,** C05027, doi:10.1029/2007JC004477.

Knight, J. R., R. J. Allan, C. K. Folland, M. Vellinga, and M. E. Mann, 2005: A signature of persistent natural thermohaline circulation cycles in observed climate. *Geophys. Res. Lett.,* **32,** L20708, doi:10.1029/2005GL024233.

Lumpkin, R., and K. Speer, 2003: Large-scale vertical and horizontal circulation in the North Atlantic Ocean. *J. Phys. Oceanogr.,* **33,** 1902–1920.

Malanotte-Rizzoli, P., K. Hedstrom, H. Arango, and D. B. Haidvogel, 2000: Water mass pathways between the subtropical and tropical ocean in a climatological simulation of the North Atlantic Ocean circulation. *Dyn. Atmos. Oceans,* **32,** 331–371.

McCabe, G. J., M. A. Palecki, and J. L. Betancourt, 2004: Pacific and Atlantic Ocean influences on multidecadal drought frequency in the United States. *Proc. Natl. Acad. Sci. USA,* **101,** 4136–4141.

McPhaden, M. J., and D. Zhang, 2002: Slowdown of the meridional overturning circulation in the upper Pacific Ocean. *Nature,* **415,** 603–608.

——, and ——, 2004: Pacific Ocean circulation rebounds. *Geophys. Res. Lett.,* **31,** L18301, doi:10.1029/2004GL020727.

Medhaug, I., and T. Furevik, 2011: North Atlantic 20th century multidecadal variability in coupled climate models: Sea surface temperature and ocean overturning circulation. *Ocean Sci.,* **7,** 389–404.

Mignot, J., and C. Frankignoul, 2005: On the variability of the Atlantic meridional overturning circulation, the North Atlantic Oscillation, and the El Niño–Southern Oscillation in the Bergen Climate Model. *J. Climate,* **18,** 2361–2375.

Msadek, R., and C. Frankignoul, 2009: Atlantic multidecadal oceanic variability and its influence on the atmosphere in a climate model. *Climate Dyn.,* **33,** 45–62.

Otterå, O. H., H. Drange, M. Bentsen, N. G. Kvamstø, and D. Jiang, 2003: The sensitivity of the present-day Atlantic meridional overturning circulation to freshwater forcing. *Geophys. Res. Lett.,* **30,** 1898, doi:10.1029/2003GL017578.

Rowell, D. P., 2003: The impact of Mediterranean SSTs on the Sahelian rainfall season. *J. Climate,* **16,** 849–862.

——, C. K. Folland, K. Maskell, and M. N. Ward, 1995: Variability of summer rainfall over tropical North-Africa (1906–92) observations and modelling. *Quart. J. Roy. Meteor. Soc.,* **121,** 669–704.

Schott, F. A., W. Wang, and D. Stramma, 2007: Variability of Pacific subtropical cells in the 50-year ECCO assimilation. *Geophys. Res. Lett.,* **34,** L05604, doi:10.1029/2006GL028478.

——, L. Stramma, W. Wang, B. S. Giese, and R. Zantopp, 2008: Pacific subtropical cell variability in the SODA 2.0.2/3 assimilation. *Geophys. Res. Lett.,* **35,** L10607, doi:10.1029/2008GL033757.

Shay, L. K., G. J. Goni, and P. G. Black, 2000: Effects of a warm oceanic feature on Hurricane Opal. *Mon. Wea. Rev.,* **128,** 1366–1383.

Smith, T. M., and R. W. Reynolds, 2004: Improved extended reconstruction of SST (1854–1997). *J. Climate,* **17,** 2466–2477.

Stocker, T. F., A. Timmermann, M. Renold, and O. Timm, 2007: Effects of salt compensation on the climate model response in simulations of large changes of the Atlantic meridional overturning circulation. *J. Climate,* **20,** 5912–5928.

Sutton, R. T., and D. L. R. Hodson, 2005: Atlantic Ocean forcing of North American and European summer climate. *Science,* **309,** 115–118.

Taylor, K. E., R. J. Stouffer, and G. A. Meehl, 2012: An overview of CMIP5 and the experiment design. *Bull. Amer. Meteor. Soc.,* **93,** 485–498.

Terray, L., 2012: Evidence for multiple drivers of North Atlantic multi-decadal climate variability. *Geophys. Res. Lett.,* **39,** L19712, doi:10.1029/2012GL053046.

Ting, M., Y. Kushnir, R. Seager, and C. Li, 2009: Forced and internal twentieth-century SST trends in the North Atlantic. *J. Climate,* **22,** 1469–1481.

Wang, C., and S.-K. Lee, 2009: Co-variability of tropical cyclones in the North Atlantic and the eastern North Pacific. *Geophys. Res. Lett.,* **36,** L24702, doi:10.1029/2009GL041469.

——, S. K. Lee, and D. B. Enfield, 2008: Atlantic Warm Pool acting as a link between Atlantic multidecadal oscillation and Atlantic tropical cyclone activity. *Geochem. Geophys. Geosyst.,* **9,** Q05V03, doi:10.1029/2007GC001809.

——, S. Dong, and E. Munoz, 2010: Seawater density variations in the North Atlantic and the Atlantic meridional overturning circulation. *Climate Dyn.,* **34,** 953–968.

——, ——, A. T. Evan, G. R. Foltz, and S.-K. Lee, 2012: Multidecadal covariability of North Atlantic sea surface temperature, African dust, Sahel rainfall, and Atlantic hurricanes. *J. Climate,* **25,** 5404–5415.

——, L. Zhang, and S.-K. Lee, 2013: Response of freshwater flux and sea surface salinity to variability of the Atlantic warm pool. *J. Climate,* **26,** 1249–1267.

Zhang, D., M. J. McPhaden, and W. E. Johns, 2003: Observational evidence for flow between the subtropical and tropical Atlantic: The Atlantic subtropical cells. *J. Phys. Oceanogr.,* **33,** 1783–1797.

Zhang, L., L. Wu, and J. Zhang, 2011: Simulated response to recent freshwater flux change over the Gulf Stream and its extension: Coupled ocean–atmosphere adjustment and Atlantic–Pacific teleconnection. *J. Climate,* **24,** 3971–3988.

——, C. Wang, and L. Wu, 2012: Low-frequency modulation of the Atlantic warm pool by the Atlantic multidecadal oscillation. *Climate Dyn.,* **39,** 1661–1671.

Zhang, R., 2007: Anticorrelated multidecadal variations between surface and subsurface tropical North Atlantic. *Geophys. Res. Lett.,* **34,** L12713, doi:10.1029/2007GL030225.

——, 2010: Latitudinal dependence of Atlantic meridional overturning circulation (AMOC) variations. *Geophys. Res. Lett.,* **37,** L16703, doi:10.1029/2010GL044474.

——, and Coauthors, 2013: Have aerosols caused the observed Atlantic multidecadal variability? *J. Atmos. Sci.,* **70,** 1135–1144.